

Planar Cell Polarity (PCP) Protein Vangl2 Regulates Ectoplasmic Specialization Dynamics via Its Effects on Actin Microfilaments in the Testes of Male Rats

Haiqi Chen, Dolores D. Mruk, Will M. Lee, and C. Yan Cheng

The Mary M. Wohlford Laboratory for Male Contraceptive Research (H.C., D.D.M., C.Y.C.), Center for Biomedical Research, Population Council, New York, New York 10065; and School of Biological Sciences (W.M.L.), University of Hong Kong, Pokfulam, Hong Kong, China

Planar cell polarity (PCP) proteins confer polarization of a field of cells (eg, elongating/elongated spermatids) within the plane of an epithelium such as the seminiferous epithelium of the tubule during spermatogenesis. In adult rat testes, Sertoli and germ cells were found to express PCP core proteins (eg, Van Gogh-like 2 [Vangl2]), effectors, ligands, and signaling proteins. Vangl2 expressed predominantly by Sertoli cells was localized at the testis-specific, actin-rich ectoplasmic specialization (ES) at the Sertoli-spermatid interface in the adluminal compartment and also Sertoli-Sertoli interface at the blood-testis barrier (BTB) and structurally interacted with actin, N-cadherin, and another PCP/polarity protein Scribble. Vangl2 knockdown (KD) by RNA interference in Sertoli cells cultured in vitro with an established tight junction-permeability barrier led to BTB tightening, whereas its overexpression using a full-length cDNA construct perturbed the barrier function. These changes were mediated through an alteration on the organization actin microfilaments at the ES in Sertoli cells, involving actin-regulatory proteins, epidermal growth factor receptor pathway substrate 8, actin-related protein 3, and Scribble, which in turn affected the function of adhesion protein complexes at the ES during the epithelial cycle of spermatogenesis. Using Polyplus in vivo-jetPEI reagent as a transfection medium to silence Vangl2 in the testis in vivo by RNA interference with high efficacy, Vangl2 KD led to changes in F-actin organization at the ES in the epithelium, impeding spermatid and phagosome transport and spermatid polarity, meiosis, and BTB dynamics. For instance, step 19 spermatids remained embedded in the epithelium alongside with step 9 and 10 spermatids in stages IX-X tubules. In summary, the PCP protein Vangl2 is an ES regulator through its effects on actin microfilaments in the testis. (*Endocrinology* 157: 2140–2159, 2016)

During embryonic development, planar cell polarity (PCP; also referred to tissue polarity first noted in arthropods) pathway involving Wnt signaling is crucial to convergent extension during which the tissue narrows (converge) along one axis concomitant with elongation (extension) along a perpendicular axis due to polarized cell movement to generate the anteroposterior axis (1–7). PCP proteins are also essential to the development and function of the nervous system (8, 9), the kidney (10), the inner ear (11, 12), the skin (13), the female reproductive tract (14), and the heart (15) as well as endocytic vesicle-

mediated protein trafficking events (16) and cancer metastasis (17). In adults, PCP is known to maintain the polarization of a field of cells within the plane of a cell epithelium, most notably found in wing cell hair in *Drosophila*, and cell hair of the inner ear in mammals (11, 12, 18). In the testis, developing spermatids are polarized cells that are arranged in such a way that their heads point toward the basement membrane with their elongating tails toward the tubule lumen mediated through an actin-rich ultrastructure called apical ectoplasmic specialization (ES)

ISSN Print 0013-7227 ISSN Online 1945-7170

Printed in USA

Copyright © 2016 by the Endocrine Society

Received November 24, 2015. Accepted March 14, 2016.

First Published Online March 18, 2016

Abbreviations: Arp3, actin-related protein 3; BTB, blood-testis barrier; CAR, coxsackievirus and adenovirus receptor; Co-IP, Coimmunoprecipitation; Ctrl, control; DAPI, 4', 6-diamidino-2-phenylindole; ES, ectoplasmic specialization; Eps8, epidermal growth factor receptor pathway substrate 8; IF, immunofluorescence; JAM-A, junctional adhesion molecule A; KD, knockdown; KO, knockout; PCP, planar cell polarity; RNAi, RNA interference; siRNA, small interfering RNA; S/N, supernatant; TER, transepithelial electrical resistance; TJ, tight junctions; Vangl, Van Gogh-like protein; ZO-1, zonula occludens-1.

(19, 20), analogous to a field of polarized cells within the plane of the epithelium of the seminiferous tubule, implicating the plausible involvement of PCP proteins. Nonetheless, studies have shown that spermatid polarity and adhesion are regulated by the polarity protein complexes such as Par- and Scribble-based complexes at the apical ES (21–23) that are known to confer apicobasal polarity in other epithelia (19, 24) through their effects on the F-actin-based cytoskeleton in Sertoli cells (21, 23). On the other hand, the blood-testis barrier (BTB) at the Sertoli cell-cell interface near the basement membrane is constituted by a similar ultrastructure known as basal ES, coexisting with tight junctions (TJ) and gap junctions (25). Furthermore, Par- and Scribble-based polarity proteins are involved in conferring spermatid and Sertoli cell polarity and also spermatid and Sertoli cell adhesive function (21, 23). Yet there are no reports in the literature that examine the presence of PCP proteins in the testis and whether they are involved in ES function.

Studies have shown that PCP proteins are well conserved and found from flies to mammals. PCP proteins are classified into PCP core proteins (eg, Van Gogh-like protein, Frizzled proteins, and Dishevelled segment polarity proteins), effectors (eg, Fuzzy planar cell polarity proteins), ligands (eg, Wnt5a, tyrosine protein kinase Ror2), and signaling proteins (eg, Fat and Dachsous cadherin-related proteins). One of the best studied PCP core proteins is Van Gogh-like protein (*Vangl*), which is a homolog of Van Gogh, also known as strabismus (or FlyBase), first found in *Drosophila* (26), and also known as Ltap in the mouse based on a neural tube mutant loop tail mouse model (27). Two *Vangl* homologs are found in mammalian cells: *Vangl1* and *Vangl2*, with about 70% similarity in their polypeptide sequences and identical predicted secondary structures. Mutation of either *Vangl1* (28–30) or *Vangl2* (29, 31, 32) in humans lead to neural tube defects. Interestingly, although *Vangl2* knockout (KO) mice are not viable due to neural tube defects, leading to embryonic fatality (27, 33), and *Vangl2* mutation in mice also leads to failure in lung and kidney development (34), neural tube defects found in *Vangl1*-inactivated mice are less severe (35, 36). Collectively these findings suggest that *Vangl2* is playing a predominant role in development in addition to brain formation (37). Furthermore, studies have shown that *Vangl2*, a small integral membrane protein with four-transmembrane domains, is involved in the assembly and maintenance of adherens junction in the brain and kidney (38–40), and changes in its expression level via RNA interference (RNAi) or overexpression in epithelial cell lines human embryonic kidney-293T and MDCK were shown to perturb cell-cell and cell-substratum adhesion mediated through changes in cytoskeletal

function (41). Based on this information, we elected to examine whether *Vangl2* was involved in spermatogenesis. It is obvious that studies will be expanded to cover *Vangl1* and other pertinent PCP proteins in future investigations.

Materials and Methods

Animals

The use of animals (Sprague Dawley male pups and adult rats; Charles River Laboratories) for all the experiments reported herein was approved by The Rockefeller University Institutional Animal Care and Use Committee with protocol numbers 12-506 and 15-780-H.

Primary Sertoli cell cultures

Sertoli cell cultures were prepared using cells isolated from 20-day-old rat testes as described (42). Cells were plated at Matrigel (BD Biosciences)-coated dishes, bicameral units, or cover glasses (round, 18 mm diameter) at different densities optimized for specific experiments based on pilot experiments as follows. For the preparation of cell lysates for immunoblotting and actin bundling assays, Sertoli cells were plated at 0.4×10^6 cells/cm² on 12- and six-well dishes containing 3 and 5 mL F12/DMEM, respectively. For transepithelial electrical resistance (TER) measurements to monitor the Sertoli cell TJ-permeability barrier function, Sertoli cells were plated at 1.2×10^6 cells/cm² on Millipore Millicell HA (mixed cellulose esters) culture plate inserts (diameter 12 mm; effective surface area ~ 0.6 cm²). Inserts were placed in 24-well dishes, with each insert containing 0.5 mL F12/DMEM in the apical and basal chamber, respectively. For immunofluorescence (IF) or dual-labeled IF analysis, Sertoli cells were cultured at 0.04×10^6 cells/cm² on microscopic cover glasses, and cover glasses were placed on 12-well dishes, with each well containing 2 mL F12/DMEM.

Knockdown (KD) of *Vangl2* by RNAi

Studies *in vitro*

For *Vangl2* KD, primary Sertoli cells were transfected with Silencer Select Negative Control No.1 small interfering RNA (siRNA; Ambion-Life Technologies) (Ctrl) duplexes vs Silencer Select siRNA duplexes specifically targeting rat *Vangl2* (s144160 and s144162; Ambion-Life Technologies) at 100 nM using Lipofectamine RNAiMax (Invitrogen-Life Technologies) as a transfection medium on day 2. Transfection reagents and siRNA duplexes were removed 24 hours later (ie, d 3), and cells were rinsed in F12/DMEM and cultured in fresh F12/DMEM for 12 hours to allow recovery. Thereafter, cells were subject to another transfection for 24 hours. Twelve hours after the second transfection, cells were harvested and used for immunoblotting, actin bundling assay, or IF analysis except for experiments that monitored the TJ-barrier function. TER reading was obtained daily from each bicameral unit until day 8. We elected to transfect cells twice for double KD based on results of pilot experiments because a single KD led to a down-regulation of *Vangl2* expression by approximately 50% vs an approximately 70%–80% after a double KD when examined by immunoblotting and

reported herein. The sequences of the two pairs of Vangl2 siRNA duplexes used were as follows: sense, 5'-GGCACUUCU GAGCACAGUAtt-3', antisense, 5'-UACUGUGCUCAGAAGU GCCtg-3' (s144160); and sense, 5'-AGGAAUUCGUGGAUC CCAAtt-3', antisense, 5'-UUGGGAUCCACGAAUUCUcg-3' (s144162). For IF cell staining, siGLO red transfection indicator (Dharmacon-GE Healthcare) was cotransfected with either negative Ctrl or Vangl2 siRNA duplexes at a final concentration of 1 nM to monitor relative transfection efficiency.

Studies in vivo

For Vangl2 RNAi in vivo, siRNA duplexes were suspended in 35 μ L sterile 5% glucose (wt/vol) and mixed with in vivo-jetPEI reagent (Polyplus) (at 0.16 μ L in vivo-jetPEI reagent per μ g siRNA duplexes; ie, 0.27 μ L for Vangl2 siRNA duplexes vs 0.32 μ L for the negative control siRNA duplexes, suspended in 35 μ L 5% glucose) at room temperature to a final transfection mix volume of 70 μ L for each testis (assuming a volume of ~1.6 mL per testis) containing siRNA duplexes at 100 nM for either Ctrl or Vangl2 RNAi group. In short, the right testis of the same rat received 70 μ L of control transfection mix containing the non-targeting negative control duplexes vs the left testis receiving the same volume of transfection mix that contained the Vangl2 siRNA duplexes with six rats. Transfection mix was loaded into the testis via intratesticular injection as described (43). A total of two transfections were performed, with the first transfection on day 1 and the second on day 5 to maximize Vangl2 KD. Rats were euthanized on day 8 by CO₂ asphyxiation using slow (20%–30%/min) displacement of chamber air from a compressed CO₂ tank.

Preparation of a full-length Vangl2 cDNA and its overexpression using a mammalian expression vector pCI-neo

Cloning of the Vangl2 full-length cDNA was performed as earlier described for focal adhesion kinase (44) and rpS6 (45). In brief, cDNAs were obtained from 20-day-old Sertoli cells cultured for 2 days as described (44), which served as the template for cloning by PCR. A 1566-bp rat (*Rattus norvegicus*) Vangl2 full-length cDNA (Genbank accession number NM_001105969) containing the start and stop codons as well as the open reading frame was obtained by PCR using AccuPrime Taq DNA polymerase high fidelity (Invitrogen-Life Technologies) and a primer pair specific to rat Vangl2 flanked by *Mlu*I and *Xba*I cloning sites at the corresponding 5'- and 3'-end (Supplemental Table 1). This clone was confirmed by direct nucleotide sequencing at Genewiz and cloned into the pCI-neo mammalian expression vector (Promega). Plasmid DNA was treated with the MiraCLEAN endotoxin removal kit (Mirus) before transfection. Sertoli cells cultured in vitro for 2 days were used for overexpression in which cells were transfected with either empty vector (pCI-neo) or plasmid DNA containing the full-length Vangl2 cDNA (pCI-neo/Vangl2) using 0.5 μ g plasmid DNA per 1×10^6 Sertoli cells (in ~0.5 mL F12/DMEM) using a K2 Transfection Reagent (K2 transfection system, Biontex) for 14 hours. Thereafter, cells were rinsed with F12/DMEM twice and cultured in fresh F12/DMEM for an additional 36 hours. Cells were terminated on day 4 to obtain lysate for immunoblotting and actin bundling assay or

fixed and processed for IF. Plasmid DNA was labeled with Cy3 using a LabelIT Tracker intracellular nucleic acid localization kit (Mirus) to confirm successful transfection.

IF and dual-labeled IF analysis

IF was performed (44, 45) using corresponding primary and secondary antibodies (Table 1). For F-actin staining, either an anti-actin antibody (Table 1) or fluorescein isothiocyanate-conjugated phalloidin (Invitrogen-Life Technologies) was used. Nuclei were visualized with 4', 6-diamidino-2-phenylindole (DAPI). Images were obtained using an Olympus BX61 fluorescence microscope with a built-in Olympus DP-71 digital camera, and images were acquired using the Olympus MicroSuite Five software package (version 1224). Images were analyzed using Adobe Photoshop such as for image overlay. After the overexpression of Vangl2 by transfecting Sertoli cells with the Vangl2 full-length cDNA or its KD by RNAi, changes in fluorescence intensity were monitored by Image J (<http://imagej.nih.gov/ij/>) (46), and changes in protein distribution at the cell-cell interface were quantified by measuring the distance redistributed from the cell-cell interface as described (43, 46). In brief, fluorescence intensity and the width of fluorescence at the cortical zone at four opposite ends between adjacent cells were assessed, and 50 randomly selected pairs of cells were analyzed from three independent experiments.

Coimmunoprecipitation (Co-IP)

Co-IP using testes lysates (1 mg protein) was performed as detailed elsewhere (44, 45, 47). In some experiments, possible interaction between Vangl2 and its target proteins (eg, N-cadherin, actin) was assessed using lysates (400 μ g protein) of Sertoli cells (0.4×10^6 cells/cm²), overexpressed with Vangl2 on day 2 with pCI-neo/Vangl2 vs pCI-neo empty vector (Ctrl) for 14 hours and terminated on day 4 to better identify binding partner proteins. Lysates of testes and Sertoli cells were obtained as earlier described (44, 45) using IP lysis buffer (50 mM Tris-HCl, containing 1% Nonidet P-40, 150 mM NaCl, 2 mM EGTA, and 10% glycerol [pH 7.4] at 22°C, supplemented with protease and phosphatase inhibitors cocktails from Sigma-Aldrich). In brief, lysates of adult rat testes (1 mg protein per sample) or Sertoli cells (400 μ g protein per sample) were incubated with a primary antibody (2 μ g IgG) vs normal IgG (2 μ g, served as a control) of the corresponding animal species in a final volume of approximately 250 μ L either for 36 hours (testis lysates) or overnight (Sertoli cell lysates) at 4°C with agitation. Thereafter, 20 μ L of Protein A/G Plus-agarose (Santa Cruz Biotechnology) was added to the antigen-antibody complex suspension above and incubated for approximately 6 hours at 4°C on a rocking platform. Immunocomplexes were obtained and separated from other unbound proteins by centrifugation (1000 $\times g$, 5 min at 4°C) and washed four times with IP lysis buffer. Immunocomplexes were extracted from the Protein A/G Plus-agarose using sodium dodecyl sulfate sample buffer (0.125 M Tris; 1% sodium dodecyl sulfate; 1.6% β -mercaptoethanol; 20% glycerol [vol/vol], pH 6.8 at 22°C) at 100°C for 10 minutes and analyzed by immunoblotting using corresponding specific antibodies (Table 1) to identify the binding partners of Vangl2. To further confirm specific interaction between Vangl2 and Scribble, anti-Scribble IgG was also used as an immunoprecipitating antibody to pull out Vangl2 proteins in

Table 1. Antibodies Used for Different Experiments in This Report

Antibody	Host Species	Vendor	Catalog Number	Application (Dilution)
Actin	Goat	Santa Cruz Biotechnology	sc-1616	IB (1:200), IP (1:25)
Actin	Rabbit	Cytoskeleton	AAN01	IF-paraffin section (1:100)
Arp3	Mouse	Sigma-Aldrich	A5979	IB (1:3000), IF tissue (1:200), IF cell (1:50), IP (1:250)
β 1-Integrin	Goat	Santa Cruz Biotechnology	sc-6622	IF (1:100)
β -Catenin	Mouse	Invitrogen-ThermoFisher Scientific	138400	IB (1:300), IF (1:100)
CAR	Rabbit	Santa Cruz Biotechnology	sc-15405	IB (1:200)
Claudin-11	Rabbit	Invitrogen-ThermoFisher Scientific	36-4500	IB (1:200), IF (1:100)
Drebrin E	Rabbit	Abcam	ab11068	IB (1:1000)
Eps8	Mouse	BD Biosciences	610143	IB (1:5000), IF tissue (1:100), IF cell (1:50), IP (1:30)
E-cadherin	Rabbit	Santa Cruz Biotechnology	sc-7870	IB (1:150)
JAM-A	Rabbit	Invitrogen-ThermoFisher Scientific	361700	IB (1:150)
Laminin- γ 3	Rabbit	Cheng Lab		IF (1:300)
N-cadherin	Mouse	Invitrogen-ThermoFisher Scientific	33-3900	IB (1:200), IF (1:100), IP (1:60)
Nectin-3	Goat	Santa Cruz Biotechnology	sc-14806	IF (1:100)
Occludin	Rabbit	Invitrogen-ThermoFisher Scientific	711500	IB (1:250)
Scribble	Goat	Santa Cruz Biotechnology	sc-11048	IB (1:500), IF (1:100), IP (1:25)
Scribble	Rabbit	Cell Signaling Technology	4475	IF-paraffin section (1:100)
Vangl2	Sheep	R&D Systems	AF4815	IF-paraffin section (1:100)
Vangl2	Goat	Santa Cruz Biotechnology	sc-46561	IB (1:500), IF cell (1:50), IP (1:25)
Vangl2	Rabbit	Sigma Aldrich	HPA027043	IB (1:200) (after Co-IP)
ZO-1	Rabbit	Invitrogen-ThermoFisher Scientific	61-7300	IB (1:250), IF (1:100)
Mouse IgG secondary antibody, Alexa Fluor 555	Donkey	Invitrogen-ThermoFisher Scientific	A-31570	IF tissue (1:250), IF cell (1:100)
Rabbit IgG secondary antibody, Alexa Fluor 555	Donkey	Invitrogen-ThermoFisher Scientific	A-31572	IF tissue (1:250), IF cell (1:100)
Sheep IgG secondary antibody, Alexa Fluor 488	Donkey	Invitrogen-ThermoFisher Scientific	A-11015	IF tissue (1:250)
Goat IgG secondary antibody, Alexa Fluor 488	Donkey	Invitrogen-ThermoFisher Scientific	A-11055	IF tissue (1:250), IF cell (1:100)
Goat IgG secondary antibody, Alexa Fluor 555	Donkey	Invitrogen-ThermoFisher Scientific	A-21432	IF tissue (1:250), IF cell (1:100)
Rabbit IgG Secondary Antibody, Alexa Fluor 488	Donkey	Invitrogen-ThermoFisher Scientific	A-21206	IF tissue (1:250), IF cell (1:100)
Mouse IgG Secondary Antibody, Alexa Fluor 488	Donkey	Invitrogen-ThermoFisher Scientific	A-21202	IF tissue (1:250), IF cell (1:100)
Goat IgG Secondary Antibody, HRP	Bovine	Santa Cruz Biotechnology	sc-2350	IB (1:3000)
Rabbit IgG secondary antibody, HRP	Bovine	Santa Cruz Biotechnology	sc-2370	IB (1:3000)
Mouse IgG secondary antibody, HRP	Bovine	Santa Cruz Biotechnology	sc-2371	IB (1:3000)

Abbreviations: HRP, horseradish peroxidase; IB, immunoblotting; IP, immunoprecipitation.

testis lysates in which normal goat IgG served as the negative control, and anti-Vangl2 IgG that pulled out Vangl2 served as the positive control. To assess the validity of Co-IP, an aliquot (20 μ L) of supernatant from each reaction tube in the Co-IP experiment, using anti-Scribble IgG for Co-IP and after immunocomplexes were precipitated by Protein A/G-Plus agarose, was withdrawn and subjected to immunoblot analysis using an anti-Scribble antibody. This thus verified whether Scribble protein was pulled out by anti-Scribble IgG vs anti-Vangl2 IgG and normal IgG (control) to further confirm Scribble was a binding partner of Vangl2. The host species of all antibodies used for Co-IP and immunoblotting was indicated.

Actin bundling assay, immunoblotting, and RT-PCR

Actin bundling assay was performed essentially as earlier described (48). Immunoblotting was performed as described (49). About 15–50 μ g protein of Sertoli cell lysates or approximately 70 μ g protein of testis lysates were used. Antibodies used for Co-IP and immunoblotting are listed in Table 1. RNA extraction and PCR were performed as described (43) using primers specific to different target genes listed in *Supplemental Table 1*. PCR products were verified by direct DNA sequencing at Genewiz.

Histological analysis to assess the status of spermatogenesis after Vangl2 KD in adult rat testes

Histological analysis using paraffin-embedded sections stained by hematoxylin and eosin was performed as described (43). The following parameters were used to categorize defects in spermatogenesis in the Vangl2 KD testes vs control testes: 1) defects in spermatid transport across the adluminal compartment in stage VIII tubules (with more than five step 19 spermatids were detected in the epithelium of a tubule that failed to line up near the tubule lumen but embedded inside the epithelium); 2) defects in spermatid and phagosome transport in stage IX-X tubules (more than five step 19 spermatids were found in the epithelium of a tubule along with steps 9–10 spermatids and/or at least more than five phagosomes were found near the luminal edge when they should have been transported near the tubule base for degradation) (50); 3) defects in spermatid polarity in stage VII–VIII tubules (more than five spermatids that had defects in polarity in which their heads no longer pointed toward the basement membrane but at least 90° deviated from its intended orientation); and 4) defects in meiosis (the number of meiosis in the cross-section of a stage XIV tubule was scored).

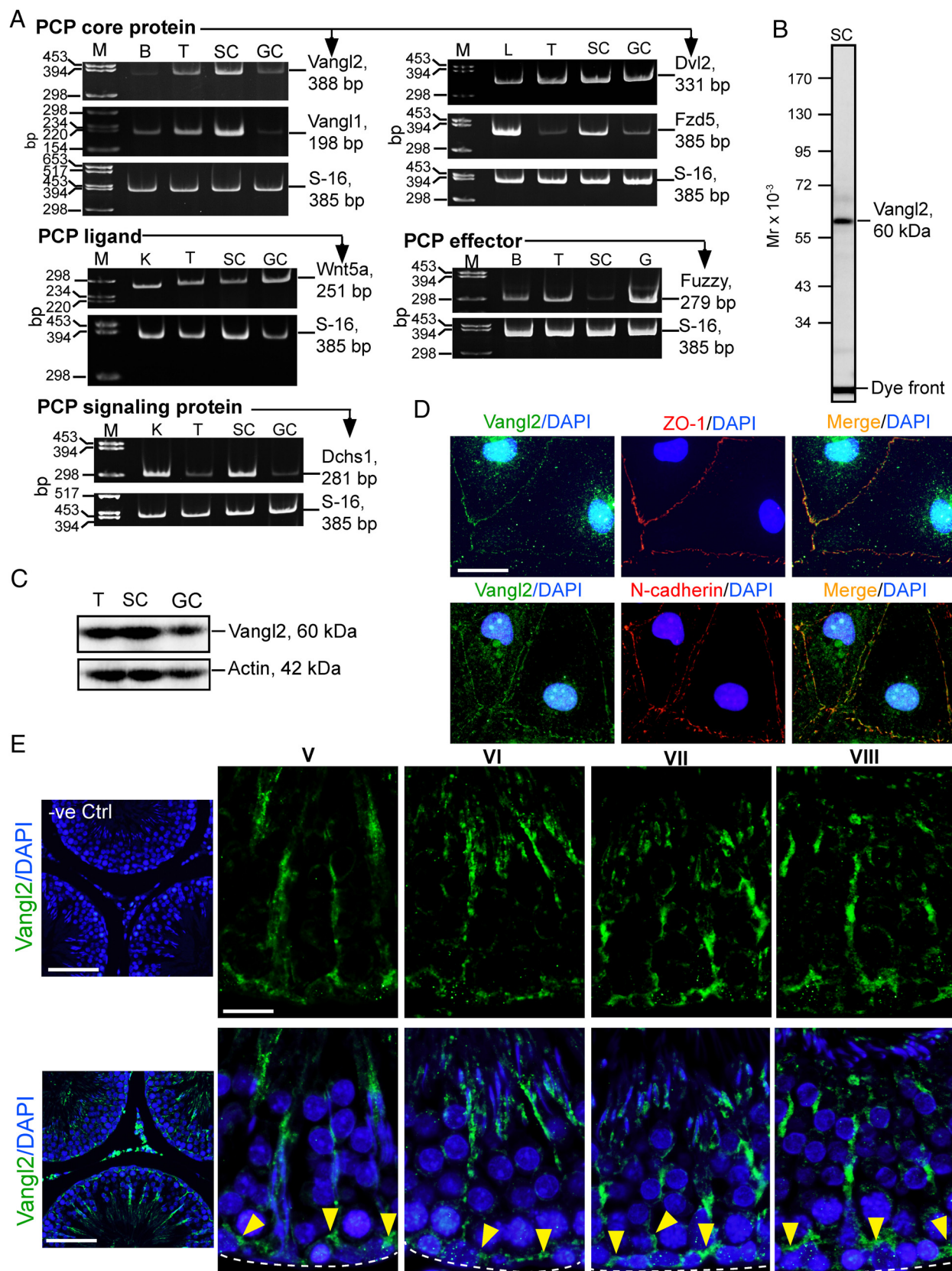


Figure 1. PCP proteins in adult rat testes, and stage-specific expression of Vangl2 in the seminiferous epithelium. A, Relative expression of PCP core proteins (eg, Vangl2, Vangl1, Dvl2 [Dishevelled 2], and Fzd5 [Frizzled class receptor 5, the receptor for the Wnt5a ligand]) vs PCP ligand (eg, Wnt5a), PCP effector (eg, Fuzzy), and PCP signaling protein (eg, Dchs1 [dachsous cadherin-related 1, a ligand of the Fat receptor]) in the testis (T), Sertoli cells (SCs; isolated from 20 d old rat testes and cultured for 4 d) and germ cells (GCs; total germ cells isolated from adult rat testes and

For this analysis, at least 100, 80, 60, and 40 stage VIII, VII, IX–X, and XIV tubules, respectively, from each rat testis of three rats were randomly selected and scored in both Vangl2 KD and control groups.

Statistical analysis

Each data point was expressed as a mean \pm SD of three independent experiments or three rats. For morphological analysis, each experiment was performed at least three times using different batches of Sertoli cells or testes from three rats. Statistical significance was evaluated with a Student's *t* test for paired comparisons.

Results

Vangl2 displays stage-specific localization in the seminiferous epithelium of adult rat testes

All the PCP core (eg, Vangl1, Vangl2, Dvl2, Fzd5), ligand (eg, Wnt5a), effector (eg, Fuzzy) and signaling (eg, Dchs1) proteins that were examined by RT-PCR using primer pairs specific to these PCP proteins (*Supplemental Table 1*) were found to be expressed in Sertoli cells, germ cells, and in adult rat testes along with the corresponding positive controls in brain, liver, or kidney (Figure 1A). The identity of the corresponding PCP cDNA obtained by PCR was confirmed by direct nucleotide sequence analysis at Genewiz, which matched the Genbank database (see *Supplemental Table 1*). Specificity of the Vangl2 antibody (Table 1) used for our studies was demonstrated by immunoblotting, using lysates from Sertoli cells (Figure 1B).

Figure 1. (Continued). cultured for ~16 h) including other positive controls, such as brain (B), liver (L), and kidney (K) by RT-PCR with S16 as a PCR/loading control using specific primer pairs for the corresponding target genes (see *Supplemental Table 1*). M, DNA size marker in base pairs. B, Immunoblotting of Sertoli cell lysate probed with an anti-Vangl2 antibody (see Table 1), with PageRuler prestained protein markers (CrystaGen, Inc) on the left. Mr, molecular weight. C, Immunoblotting of lysates of adult rat testes (T), SCs, and GCs using an anti-Vangl2 antibody. D, Localization of Vangl2 (green fluorescence) in Sertoli cells and its colocalization with ZO-1 (red fluorescence, upper panel) and N-cadherin (red fluorescence, lower panel) at the cell-cell interface in cells cultured in vitro. Sertoli cell nuclei were visualized by DAPI (blue). Scale bar, 20 μ m, which applies to other micrographs. E, IF staining was performed by using paraffin sections of paraformaldehyde-fixed adult rat testes and an anti-Vangl2 antibody (Table 1). Vangl2 localized to the BTB/basal ES (annotated by yellow arrowheads, and the relative location of the basement membrane was annotated by a dashed white line) and apical ES stage specifically. Vangl2 was visualized with Alexa Fluor 488 (green fluorescence). Nuclei were visualized with DAPI (blue fluorescence). Negative control (–ve Ctrl) (top left panel) was performed in which the sheep anti-Vangl2 antibody was replaced by normal sheep IgG at similar concentration with the primary antibody and yielded negligible staining vs the sheep anti-Vangl2 IgG (bottom left panel). Stages of the seminiferous epithelial cycle are noted as roman numerals (four right panels). Scale bar, 350 μ m, for –ve Ctrl and corresponding Vangl2 staining; 40 μ m, which applies to other micrographs.

Sertoli cells were found to express more Vangl2 vs germ cells when the steady-state protein level of Vangl2 in lysates of Sertoli cells, germ cells, and testes was assessed and compared by immunoblotting (Figure 1C), consistent with findings of RT-PCR (Figure 1A vs. 1C). When Sertoli cells were cultured in vitro for 4 days to form an intact epithelium, Vangl2 was detected at the cell-cell interface, colocalized with a TJ adaptor protein zonula occludens-1 (ZO-1) and basal ES protein N-cadherin, some Vangl2 protein was also detected in cell cytosol and nucleus (Figure 1D). This pattern of localization in the Sertoli cell epithelium is consistent with findings in other mammalian cells, such as COS-7 cells (a fibroblast-like cell line derived from monkey kidney tissue) and mouse cochlear cells (51).

In the seminiferous epithelium of adult rat testes, negative control (–ve Ctrl), wherein the sheep anti-Vangl2 IgG (Table 1) was replaced by normal sheep IgG, yielded negligible fluorescence staining (Figure 1E, left panel), illustrating the specificity of Vangl2 staining shown in Figure 1E (see four right panels). Immunoreactive Vangl2 was localized predominantly at the BTB/basal ES and the apical ES and was expressed stage specifically (Figure 1E). For instance, Vangl2 was found at or near the BTB in stages V–VI of the epithelial cycle but most prominently at stages VII–VIII when the BTB undergoes restructuring to accommodate the transport of preleptotene spermatocytes at these stages (see yellow arrowheads in Figure 1E). Some stalk-like ultrastructures typical of Sertoli cell cytoplasmic processes were also noted in the seminiferous epithelium (Figure 1E). However, Vangl2 diminished to an almost undetectable level at the BTB at stage IX, which persisted through stage IV until it was expressed again at stage V. At the apical ES, Vangl2 was expressed from stages V to IX with the strongest expression at V–VII, covering the front end of spermatid heads, but its expression diminished considerably by stage VIII (Figure 1E).

Vangl2 is a component of the apical ES and basal ES/BTB in adult rat testes

To further investigate the precise localization of Vangl2 in the seminiferous epithelium of rat testes, a dual-labeled IF analysis was performed (Figure 2, A and B). Vangl2 was found to colocalize, at least in part, with F-actin and two putative apical ES-associated actin regulatory proteins actin-related protein 3 (Arp3; a branched actin nucleation protein which together with Arp2 forms the Arp2/3 complex capable of inducing actin microfilament branching, causing debundling/branching of bundled filaments [52]) and epidermal growth factor receptor pathway substrate 8 (Eps8) (an actin barbed end capping and bundling protein that confers actin microfilaments a bundled configuration [53]) at the concave (ventral) side of spermatid

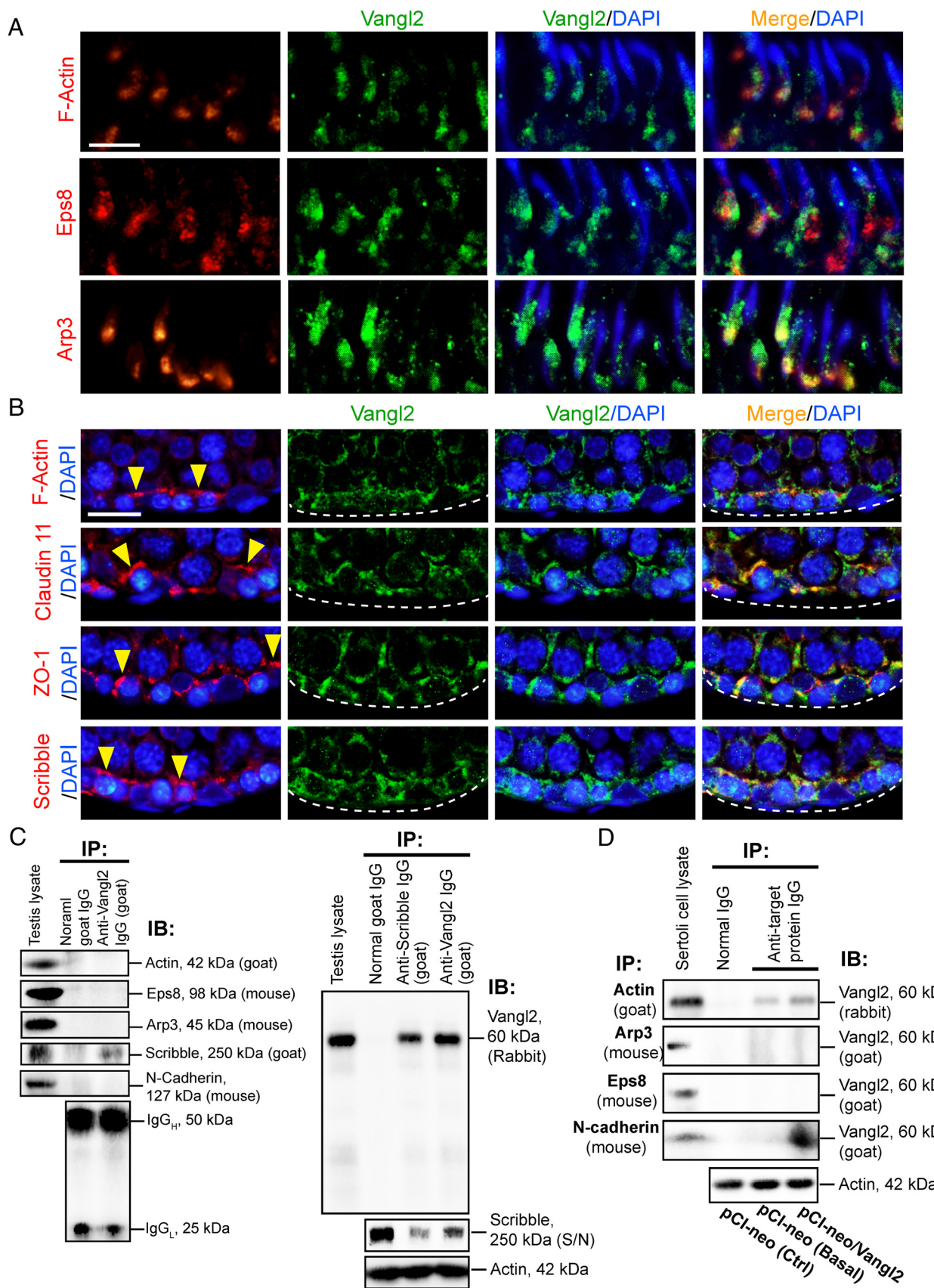


Figure 2. Colocalization and interactions of Vangl2 with BTB-associated proteins in the testis or Sertoli cells cultured in vitro with an established functional TJ-permeability barrier. A, Colocalization of Vangl2 (green fluorescence) with F-actin (red fluorescence) and the actin-regulatory proteins Eps8 (red fluorescence, an actin barbed end capping and bundling protein) and Arp3 (red fluorescence, a branched actin polymerization protein by

heads (Figure 2A), consistent with its localization at the apical ES, which was transformed to an ultrastructure known as the apical tubulobulbar complex at late stage VII, representing a giant endocytic vesicle to accommodate the endocytosis and recycling of apical ES proteins for the assembly of new apical ES when step 8 spermatids form at stage VIII before it was degenerated prior to the release of sperms at spermiation (54–56).

At the basal ES/BTB, Vangl2 also colocalized with F-actin, TJ-integral membrane protein claudin 11, TJ-adaptor protein ZO-1, and polarity protein Scribble, which is known to regulate F-actin organization and also a component of the basal ES/BTB (23) (Figure 2B). Interestingly,

Figure 2. (Continued). converting a linear actin microfilament to a branched configuration via barded end nucleation) at the apical ES in the seminiferous epithelium of adult rat testes using paraffin sections fixed in paraformaldehyde. Scale bar, 20 μ m, which applies to other micrographs. B, Colocalization of Vangl2 (green) with F-actin (red), TJ integral membrane protein claudin 11 (red), TJ adaptor protein ZO-1 (red), and polarity protein Scribble (red) at the basal ES/BTB in adult rat testes. Nuclei were visualized with DAPI (blue fluorescence). The relative location of basement membrane was annotated by a dashed white line, and the BTB was annotated by yellow arrowheads. Scale bar, 40 μ m, which applies to other micrographs. C, Co-IP using testis lysates (~1 mg of protein per lane) was performed using a goat anti-Vangl2 antibody (see Table 1) vs normal goat IgG (control), and the binding partner proteins in the pulled-out immunocomplexes were identified using corresponding specific antibodies against actin, actin regulatory proteins Eps8 and Arp3, and other BTB-associated proteins Scribble and N-cadherin (animal species used to generate the antibody were annotated). Vangl2 was found to interact with Scribble, but not actin, Eps8, Arp3, and N-cadherin (left panel), using testis lysates with normal goat IgG served as the negative control, and testis lysate at 40 μ g protein without Co-IP served as the corresponding positive control. Specific interaction of Vangl2 with Scribble was confirmed by pulling out Vangl2 using an anti-Scribble antibody as shown in the right panel with approximately 1 mg testis lysate protein per sample for Co-IP, in which anti-Vangl2 antibody or normal goat IgG served as the corresponding positive and negative control. Specificity of the Co-IP shown herein was further confirmed by quantifying the amount of remaining Scribble in the S/N not pulled down in the immunocomplexes by protein A/G Plus to illustrate considerable amount of Scribble was associated with Vangl2 (see right lane in the lower panel immunoprecipitated with a goat anti-Vangl2 antibody, which had considerable less Scribble vs the amount of Scribble in the left lane immunoprecipitated with normal goat IgG, and considerably fewer Scribble was found in the sample immunoprecipitated with a goat anti-Scribble antibody shown in the middle lane; 20 μ L S/N from the 250- μ L sample was used for this experiment). IgG (see the denoted heavy and chains) or β -actin served as the protein loading control. IB, immunoblotting; IP, immunoprecipitation. D, Co-IP was also performed using lysates of Sertoli cells cultured in vitro with an established TJ-permeability barrier and subjected to overexpression of Vangl2 (pCI-neo/Vangl2) vs Ctrl (transfected with empty pCI-neo vector) in which one of the controls was performed with Co-IP with normal IgG whereas the other was performed with Co-IP with the corresponding immunoprecipitating antibody to assess the Vangl2-partner protein interaction at the basal level (ie, without Vangl2 overexpression). When Vangl2 was overexpressed in Sertoli cells, Vangl2 was found to interact with actin and N-cadherin but not Eps8 and Arp3. β -Actin served as the protein loading control.

whereas Vangl2 colocalized with many of the apical ES and basal ES/BTB proteins including actin in the seminiferous epithelium, studies by Co-IP showed that Vangl2 only structurally interacted with Scribble using lysates of adult rat testes (Figure 2C, left panel), and this finding was further confirmed by using an anti-Scribble antibody, which also pulled out Vangl2 (Figure 2C, right panel). The specificity of this Co-IP study was further assessed by quantifying the relative level of remaining Scribble in the supernatant (S/N), which demonstrated that Co-IP with Vangl2 indeed depleted Scribble from the S/N when compared with Co-IP with anti-Scribble IgG vs normal IgG (Figure 2C, lower right panel). Since it was reported that Vangl2 also interacted with E-cadherin using extracts of embryonic kidneys or cultured renal epithelial cells (40) as well as N-cadherin, but not β -catenin, using lysates of rat hippocampal neurons or human embryonic kidney-293T cells (39), we next performed Co-IP using lysates of cultured Sertoli cells with or without (Ctrl, Sertoli cells transfected with empty vector) overexpression of Vangl2 to pull out its interacting partner proteins. Vangl2 was found to interact structurally with actin and N-cadherin, but not Arp3 and Eps8 (Figure 2D). Taken collectively, these findings illustrate a functional relationship between PCP protein Vangl2 and polarity protein Scribble, as well as actin, and N-cadherin (Figure 2D).

PCP protein Vangl2 regulates Sertoli cell TJ-permeability barrier function in vitro through its effects on cell adhesion protein distribution at the Sertoli cell-cell interface

Given that Vangl2 is highly expressed in Sertoli cells at the ES, an actin-rich structure (57, 58) (Figures 1 and 2), it likely exerts its regulatory function via actin microfilaments. We next used an in vitro model to probe the significance of Vangl2 at the Sertoli cell basal ES/BTB. When Sertoli cells were cultured in vitro for approximately 2 days, they established a functional TJ-barrier that mimicked the BTB in vivo, with the notable presence of ultrastructures of TJ, basal ES, gap junction, and desmosome when examined by electron microscopy (59, 60). In brief, Sertoli cells were transfected with Vangl2-specific siRNA duplexes vs the nontargeting negative control siRNA duplexes on days 2 and 3.5 for 24 hours each (ie, a total of two transfections, with cells allowed to recover for 12 h in between), and cells were harvested on day 5 for RT-PCR. The mRNA level of *Vangl2* was found to be down-regulated considerably, but not *Vangl1* (Figure 3A), illustrating the specificity of Vangl2 KD.

Transfection efficiency using Lipofectamine RNAiMax (Invitrogen-Life Technologies) as a transfection medium

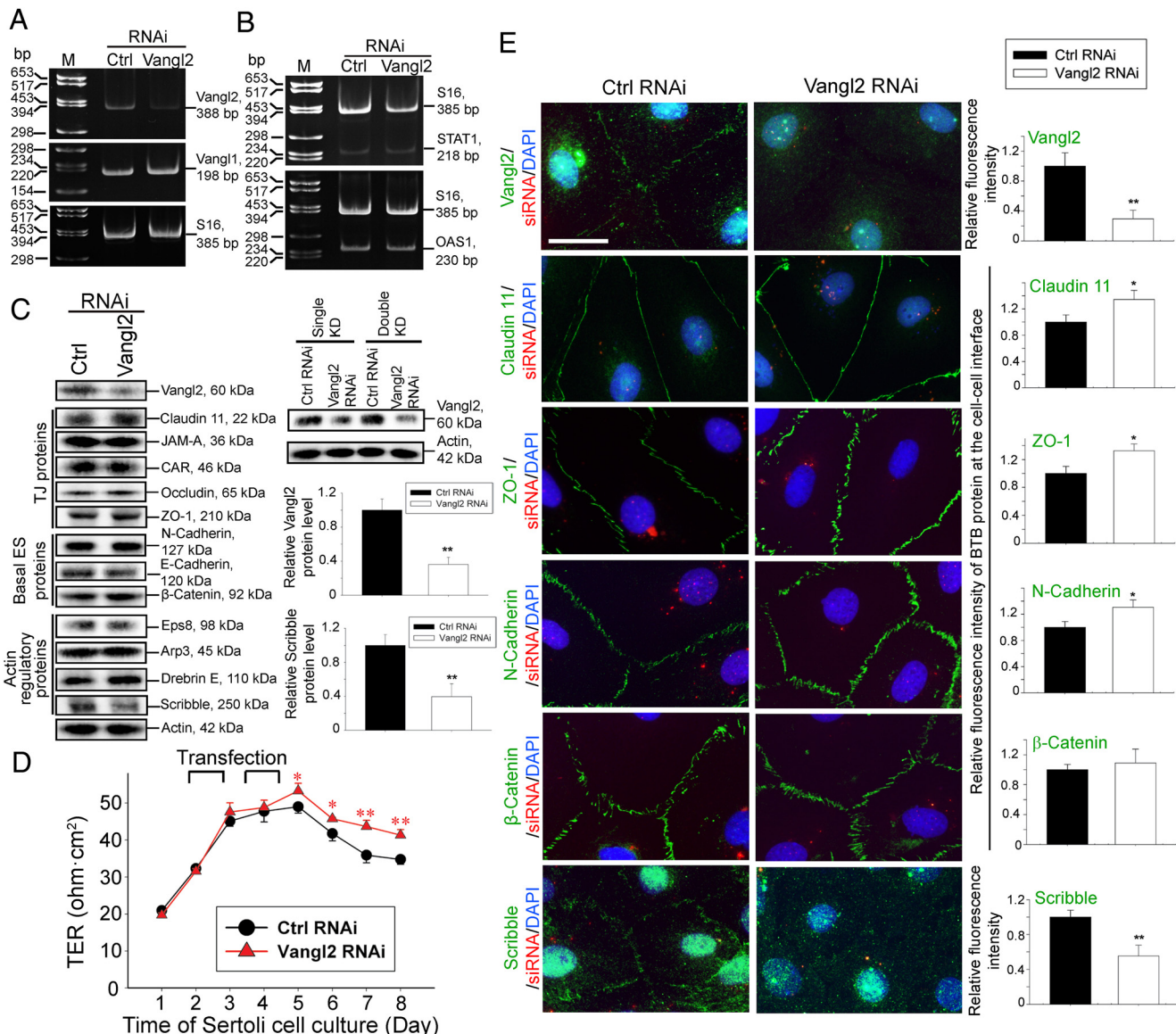


Figure 3. KD of Vangl2 at the Sertoli cells BTB in vitro enhances TJ barrier integrity through changes in the distribution of adhesion proteins at the Sertoli cell-cell interface. Sertoli cells (0.4×10^6 cells/cm²) were transfected on days 2 and 3.5 for 24 hours, respectively, with a 12-hour recovery period in between using Vangl2-specific siRNA duplexes (Vangl2 RNAi) vs nontargeting negative control siRNA duplexes (Ctrl RNAi) for efficient Vangl2 KD. Cells were then harvested on day 5 for RT-PCR, immunoblotting, and IF analysis, except for the experiment that monitored the TJ-permeability barrier by recording the TER across the cell epithelium every 24 hours, wherein Sertoli cells were kept until day 8. A, RT-PCR illustrated the steady-state level of Vangl2, but not Vangl1, mRNA reduced considerably after Vangl2 KD vs control cells, illustrating the KD specificity. B, The steady-state mRNA levels of two interferon-stimulated genes STAT1 and OAS1 remained relatively unchanged after Vangl2 KD vs control cells, supporting the notion that there were no off-target effects because STAT1 and OAS1 were earlier shown to be up-regulated when nonspecific off-target effects were detected (61, 62). C, Immunoblotting using lysates of Sertoli cells transfected with Vangl2 siRNA duplexes vs nontargeting negative control duplexes illustrates the steady-state levels of several BTB-associated proteins after Vangl2 KD. Only the steady-state level of Scribble was considerably reduced but not other proteins examined, illustrating there were no off-target effects. Immunoblots on the right panel illustrate considerably better KD efficiency was obtained in double vs single KD. Histograms on the right summarize immunoblotting results shown on the left, showing Vangl2 was silenced by approximately 70%, concomitant with a down-regulation of Scribble by 60% with a double KD. Each bar is a mean \pm SD of four experiments. **, P < .01, by Student's t test. D, Vangl2 KD in Sertoli cells (cultured at 1.2×10^6 cells/cm²) was found to tighten the Sertoli cell TJ-permeability barrier, promoting barrier function because TER across the cell epithelium was significantly higher. Each data point is a mean \pm SD of four bicameral units of an experiment, which was repeated three times using different batches of Sertoli cells and yielded similar results. *, P < .05, **, P < .01 by Student's t test. E, Relative distribution of BTB-associated proteins (green fluorescence), such as TJ proteins claudin 11 and ZO-1, basal ES proteins N-cadherin and β-catenin, and polarity protein Scribble known to regulate Sertoli cell TJ-barrier function via its effects on F-actin (23) was monitored in the Sertoli cell epithelium after Vangl2 KD vs control, and successful transfection was monitored by siGLO transfection indicator (red fluorescence) (Dharmacon-GE Healthcare). Nuclei were visualized with DAPI (blue fluorescence). Vangl2 KD induced a considerable increase in the localization of claudin 11, ZO-1, and N-cadherin, but not β-catenin, and a reduction of Scribble, at the Sertoli cell-cell interface. Scale bar, 25 μm, which applies to other micrographs. Images shown are representative findings of an experiment, and four experiments were performed using different batches of Sertoli cells and yielded similar results.

was at least 90%, based on the use of siGLO Red transfection indicator (Dharmacon-GE Healthcare) to monitor successful transfection. Because interferon-stimulated genes *STAT1* and *OAS1* were shown to be up-regulated when nonspecific off-target effects were detected (61, 62), we assessed the steady-state mRNA level of both genes by RT-PCR and detected no significant differences between the *Vangl2* RNAi and corresponding control groups (Figure 3B), illustrating *Vangl2* KD did not lead to off-target effects. Based on immunoblot analysis, the efficiency of *Vangl2* KD was at least approximately 70% (Figure 3C). *Vangl2* KD by RNAi did not significantly affect the expression of TJ (eg, claudin 11, junctional adhesion molecule A (JAM-A), coxsackievirus and adenovirus receptor (CAR), occludin, and ZO-1), basal ES (eg, N-cadherin, E-cadherin, and β -catenin) or basal ES/BTB actin regulatory proteins (eg, Eps8, Arp3, and drebrin E) (Figure 3C). However, the steady-state level of polarity protein Scribble was considerably down-regulated after *Vangl2* knockdown (Figure 3C).

Studies by immunoblotting also illustrated that a double KD was necessary (see the regimen summarized in Figure 3D) to silence *Vangl2* by approximately 70% as noted in the immunoblotting data on the right panel of Figure 3C. It was also noted that there was a tightening of the Sertoli cell permeability after *Vangl2* KD (Figure 3D), illustrating *Vangl2* KD promotes TJ-barrier function. This enhanced barrier function mediated by *Vangl2* KD might be due to the retention of claudin 11, ZO-1, and N-cadherin, but not β -catenin, to the cell-cell interface as illustrated by immunofluorescence analysis shown in Figure 3E (left panel). These observations are consistent with image analysis data when the fluorescence intensity of these proteins at the cell-cell interface was quantified (see right panel in Figure 3E). These changes in phenotypes detected in Sertoli cell cultures after *Vangl2* KD were confirmed by overexpressing *Vangl2* in Sertoli cells as shown in Figure 4, A–C. In short, *Vangl2* overexpression in Sertoli cells (Figure 4A) was found to perturb the TJ-barrier function (Figure 4B) by up-regulating the steady-state level of the actin regulatory polarity protein Scribble (Figure 4A), inducing redistribution of TJ proteins claudin-11 and ZO-1 and basal ES protein N-cadherin, but not β -catenin, causing these proteins to be rapidly internalized into the cell cytosol (Figure 4C), possibly via endocytosis, thereby

destabilizing the barrier function. Collectively these findings illustrate that *Vangl2* is a negative regulator of the BTB.

***Vangl2* regulates Sertoli cell adhesion and TJ barrier via its effects on actin organization**

PCP that confers directional cell movements require actin remodeling (63, 64), similar to spermatid transport during spermatogenesis. Thus, it is conceivable that if *Vangl2* plays a role in ES function, it likely exerts its effects through actin microfilaments because the ES is an actin-rich ultrastructure (20, 65). Indeed, after *Vangl2* KD by RNAi, actin microfilaments in Sertoli cells in the epithelium were rapidly reorganized, such that long stretches of microfilaments were lined up mostly in cell cortical zone of the Sertoli cell-cell interface (Figure 5A). However, the overall actin-bundling activity in the Sertoli cell epithelium was down-regulated (Figure 5B) because there were less actin microfilaments found across the Sertoli cell cytosol (Figure 5A). The net result of these changes thus supported the retention of adhesion proteins at the cell-cell interface, promoting the Sertoli cell TJ-barrier function as noted in Figure 3. This alteration of actin organization was mediated by changes in the spatiotemporal expression of Eps8 that confers actin microfilament bundling and branched actin polymerization inducing protein Arp3 that effectively converts linear actin microfilaments to a branched configuration via barbed end nucleation (66). For instance, more Eps8 was expressed at the Sertoli cell cortical zone with a concomitant reduction of Arp3 at or near the cell-cell interface (Figure 5A). The net result of these changes after *Vangl2* KD thus promoted Sertoli cell TJ-barrier function. Consistent with these findings, overexpression of *Vangl2*, however, disrupted actin microfilament organization in Sertoli cells, leading to truncation of actin filaments across the cell cytosol including microfilaments at the cell cortical zone (Figure 5C), even though there was an increase in actin bundling activity (Figure 5D). This alteration was also mediated by changes in the spatiotemporal expression of Eps8 and Arp3 in which considerable less Eps8 was found near the Sertoli cell cortical zone, concomitant with an increase in Arp3 at the Sertoli cell-cell interface (Figure 5C). This disorganization of actin microfilaments at the cell cortical zone after *Vangl2* overexpression thus facilitated the internalization of adhesion proteins at the Sertoli cell-cell interface, thereby destabilizing the TJ-barrier function as noted in Figure 4.

***Vangl2* KD in vivo leads to defects in spermiation by disrupting spermatid and phagosome transport and also defects in spermatid polarity in adult rat testes**

Testes transfected with siRNA duplexes to knock down *Vangl2* in vivo vs nontargeting negative control

Figure 3. (Continued). These findings are also summarized semiquantitatively in the histograms shown on the right panel. Each bar is a mean \pm SD of 25 randomly selected pairs of Sertoli cells per experiment of 3 different experiments. *, P < .01, **, P < .05 by Student's *t* test.

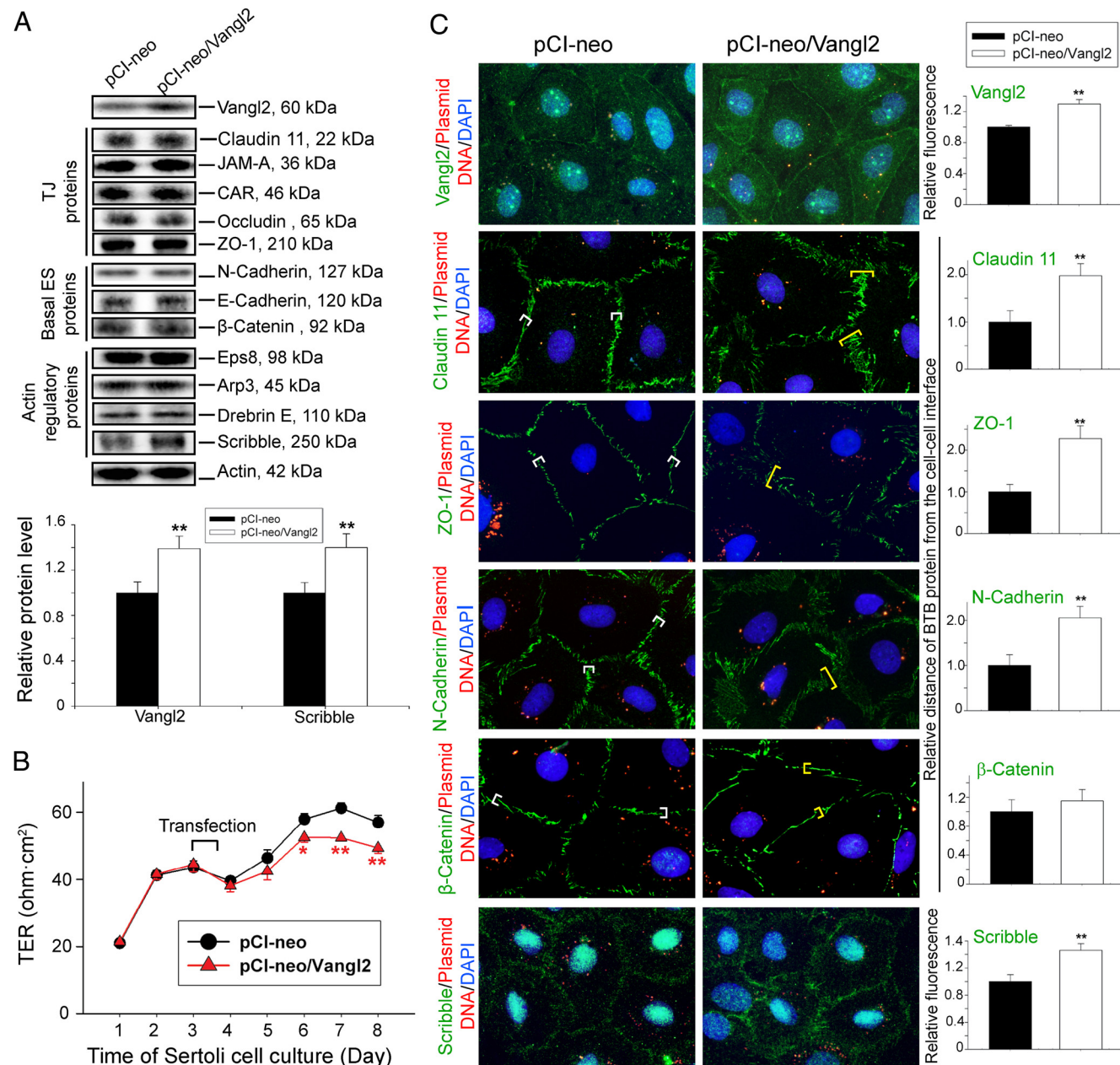


Figure 4. Overexpression of Vangl2 at the Sertoli cell BTB in vitro perturbs TJ-barrier integrity through changes in the distribution of adhesion proteins at the Sertoli cell-cell interface. For overexpression of Vangl2, Sertoli cells (0.4×10^6 cells/cm²) were transfected on day 2 with a mammalian expression vector pCl-neo containing Vangl2 cDNA (pCl-neo/Vangl2) vs empty vector (pCl-neo, control) for 14 hours, and cells were harvested on day 4 for immunoblotting and fluorescence microscopy except for the experiment that monitored the TJ-permeability barrier function wherein TER across the cell epithelium was recorded every 24 hours and Sertoli cells were kept for 8 days. A, Immunoblotting using lysates of Sertoli cells was used to assess changes in the steady-state level of multiple BTB-associated proteins after Vangl2 overexpression. An up-regulation of Scribble, but not any other proteins, was detected. Bar graph below summarizes the changes noted in the immunoblots above. Each bar is a mean \pm SD of four experiments. **, P < .01 by Student's *t* test. B, Effect of Vangl2 overexpression on the Sertoli cell TJ-permeability barrier was assessed by quantifying TER across the Sertoli cell epithelium on Matrigel-coated bicameral units with four replicate units from an experiment. Overexpression of Vangl2 perturbed the TJ-barrier function, opposite to the results of Vangl2 KD shown in Figure 3D. This experiment was repeated three times using different batches of Sertoli cells and yielded similar results. *, P < .05, **, P < .01, by Student's *t* test. C, Sertoli cells transfected with Cy3-labeled pClneo/Vangl2 (red fluorescence) for overexpression of Vangl2 vs Cy3-labeled empty vector (control) were immunostained for Vangl2, claudin-11, ZO-1, N-cadherin, β-catenin, and Scribble (green fluorescence). Nuclei were visualized with DAPI (blue fluorescence). Vangl2 was more prominent in Sertoli cell cytosol and also at the cell-cell interface following overexpression of Vangl2 when compared to control, supporting the notion that Vangl2 was successfully overexpressed in Sertoli cells. For claudin 11, ZO-1, and N-cadherin, but not β-catenin, these proteins no longer narrowly localized at the Sertoli cell-cell interface; instead, they were diffusely localized, apparently undergoing endocytosis, thereby perturbing the TJ-barrier function after Vangl2 overexpression. Scale bar, 25 μm, which applies to other micrographs. Histograms on the right summarize the results of an image analysis based on the results of the micrographs shown on the left. Each bar is a mean \pm SD of 25 randomly selected pairs of Sertoli cells per experiment with three experiments. **, P < .01 by Student's *t* test.

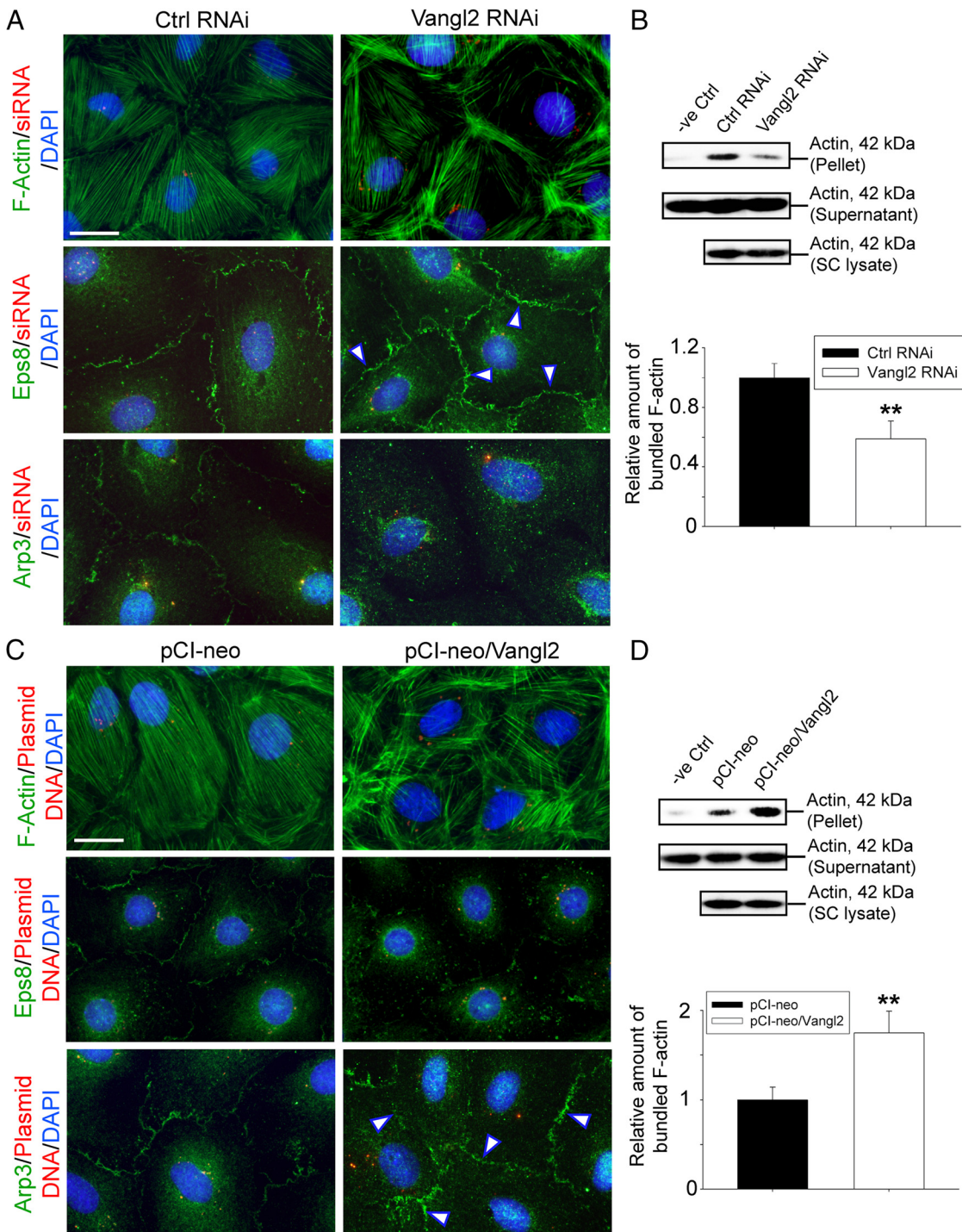


Figure 5. Changes in F-actin organization in Sertoli cells after Vangl2 KD vs overexpression are mediated through Eps8 and Arp3. F-actin was visualized using fluorescein isothiocyanate-conjugated phalloidin (green fluorescence) in Sertoli cells on day 5 or day 4 after transfection of siRNA duplexes or plasmid DNA containing Vangl2 full-length cDNA as noted in the legend to Figures 3 and 4, respectively. A, KD of Vangl2 led to the reorganization of F-actin in which microfilaments were better aligned at cell cortical zone vs control cells, thereby strengthening the Sertoli cell TJ-permeability barrier function as noted in Figure 3. This is mediated by a shift in the spatiotemporal expression of actin barded-end capping and bundling protein Eps8 and branched actin nucleation protein Arp3, in which Eps8 was more predominant at the cell-cell interface (see white arrowheads), along with a considerably reduced Arp3 localization at the cell cortical zone but more into the cell cytosol. Scale bar, 15 μ m, which applies to other micrographs. B, These results are also supported by biochemical assay that monitored the overall actin bundling activity in lysates of Sertoli cells, in which fewer actin bundles were found in these cells after Vangl2 KD because they were mostly shifted to the cell cortical zone to support the barrier function. Free actin filaments were found in supernatant, whereas bundled F-actin was concentrated in the pellet. Rabbit muscle actin incubated with only lysis buffer served as a negative control (see Materials and Methods for details). Each bar in the bottom panel of B is a mean \pm SD of three experiments, and each experiment had triplicate dishes for the bundling assay. **, P < .01 by Student's t test. C, Overexpression of Vangl2 in Sertoli cells led to the reorganization of F-actin in which microfilaments became more truncated, and a considerably

duplexes using PolyPlus in vivo-jetPEI transfection reagent, a polymer-based highly efficient transfection reagent for in vivo studies, was found to silence Vangl2 protein expression in the testis by at least 50%, without any apparent effects on BTB-associated proteins except a considerable down-regulation of Scribble expression (Figure 6A), consistent with findings in vitro (Figure 3). Vangl2 KD also induced defects in spermatogenesis in which the frequency of stage VII–VIII tubules was found to be increased by almost 1-fold to 40% in Vangl2 KD testes from 25% found in control testes, consistent with earlier findings that VII–VIII tubules accounted for about 27% of the total tubules in rats (67) (Figure 6B, upper panel). In normal rat testes, the frequency of stage IX–X tubules was at approximately 6%, also consistent with earlier data (67), but it was reduced to 4% after Vangl2 KD, a 30% reduction (Figure 6B, lower panel) due to defects in spermatid transport as noted in Figure 6C. In these tubules, spermatids were found to be pushed to undergo spermiation so that there were more apparently stage VII–VIII tubule and less stage IX–X tubules. Furthermore, those elongated spermatids (steps 18 and 19) that were inside the epithelium in stage VI and VII tubules were found to remain embedded in the seminiferous epithelium in stage VIII tubules, and many of these step 19 spermatids were persistently detected, even in stage IX and stage X tubules when elongating spermatids (steps 9 and 10) had already appeared (Figure 6, C and D). Spermatids with defects in polarity were also detected in which spermatid heads were pointing at least 90° away from the basement membrane (Figure 6C, enlarged images, red arrowheads). Addi-

tionally, phagosomes that should have been transported to the base of the seminiferous epithelium in stage IX tubules were found near the tubule lumen in this stage (Figure 6, C and D). Taken collectively, these findings confirmed defects in spermatid and phagosome transport after Vangl2 KD.

Vangl2 KD in the testis induces defects in meiosis

KD of Vangl2 was found to induce defects in meiosis (Figure 7A) because meiosis is also an actin-dependent event. The frequency of meiosis I/II found in stage XIV tubules was considerably reduced, almost by half, as noted in Figure 7, A and B, after Vangl2 KD, suggesting that the Vangl2-mediated changes in actin dynamics also perturbed meiosis.

Vangl2 regulates ES function through its effects on actin microfilaments

Apical ES

A KD of Vangl2 in the testis in vivo induced disorganization of F-actin at the apical ES in the seminiferous epithelium (Figure 8A). For instance, at the apical ES, F-actin, which was prominently localized at the concave (ventral) side of spermatid heads in control testes in stage VII tubules, was no longer tightly restricted to the spermatid head. Instead, F-actin was mostly at the convex (dorsal) side of spermatid heads (Figure 8A). Changes in F-actin organization as noted in Figure 8A that perturbed apical ES adhesion protein distribution (Figure 8B) were likely the result of changes in the spatiotemporal expression of actin barbed-end capping and bundling protein Eps8 and branched actin polymerization protein Arp3 (Figure 8A). As noted, Eps8 and Arp3 no longer restrictively localized to the concave side of spermatid heads but were considerably down-regulated or shown a lack of expression thereof in particular in spermatids displaying defects in polarity (Figure 8A). These changes in actin microfilament organization at the apical ES thus impeded the distribution of several apical ES adhesion proteins that used F-actin for their attachment. For instance, $\beta 1$ -integrin, an apical ES integral membrane protein restrictively expressed by Sertoli cells, was considerably down-regulated, and these spermatids also displayed defects in polarity with their heads no longer pointing toward the basement membrane but deviating at least 90° from the intended orientation (Figure 8B). For apical ES proteins exclusively expressed by elongated spermatids, nectin-3 was found to become considerably mislocalized, no longer tightly restricted to the convex side of spermatid heads but diffusely localized (Figure 8B); whereas laminin- $\gamma 3$ was grossly down-regulated (Figure 8B).

Figure 5. (Continued). reduced number of long stretches of actin microfilaments was found at the cell cortical zones, thereby destabilizing cell adhesion proteins to support the Sertoli cell TJ-permeability barrier function as noted in Figure 4. These changes appeared to be mediated through a shift in the spatiotemporal expression of Eps8 and Arp3 in which Eps8 at the cell-cell interface was considerably reduced, but more Arp3 was found at the cell cortical zone (see white arrowheads). Scale bar, 15 μ m, which applies to other micrographs. D, An increase in actin bundling activity was detected in lysates of Sertoli cells after overexpression of Vangl2, likely due to an increase in branched actin polymerization activity mediated by the Arp2/3 complex. In this context, it is of interest to note that the goat antihuman actin antibody used in our study (Table 1) cross-reacted with α -, β - and γ -actin in rats and rabbits; however, actin found in rat Sertoli cells is predominantly β -actin, whereas actin found in the rabbit skeletal muscle supplied in the kit is predominantly α -actin; as such, the bands shown in panels B and D were a combination of α - and β -actin, and this biochemical assay semiquantitatively assessed the ability of Sertoli cell (SC) lysates after KO and overexpression of Vangl2 to bundle α -actin supplied in the kit. Each bar is a mean \pm SD of three experiments, and each experiment had triplicate dishes for the bundling assay. **, $P < 0.01$ by Student's *t* test.

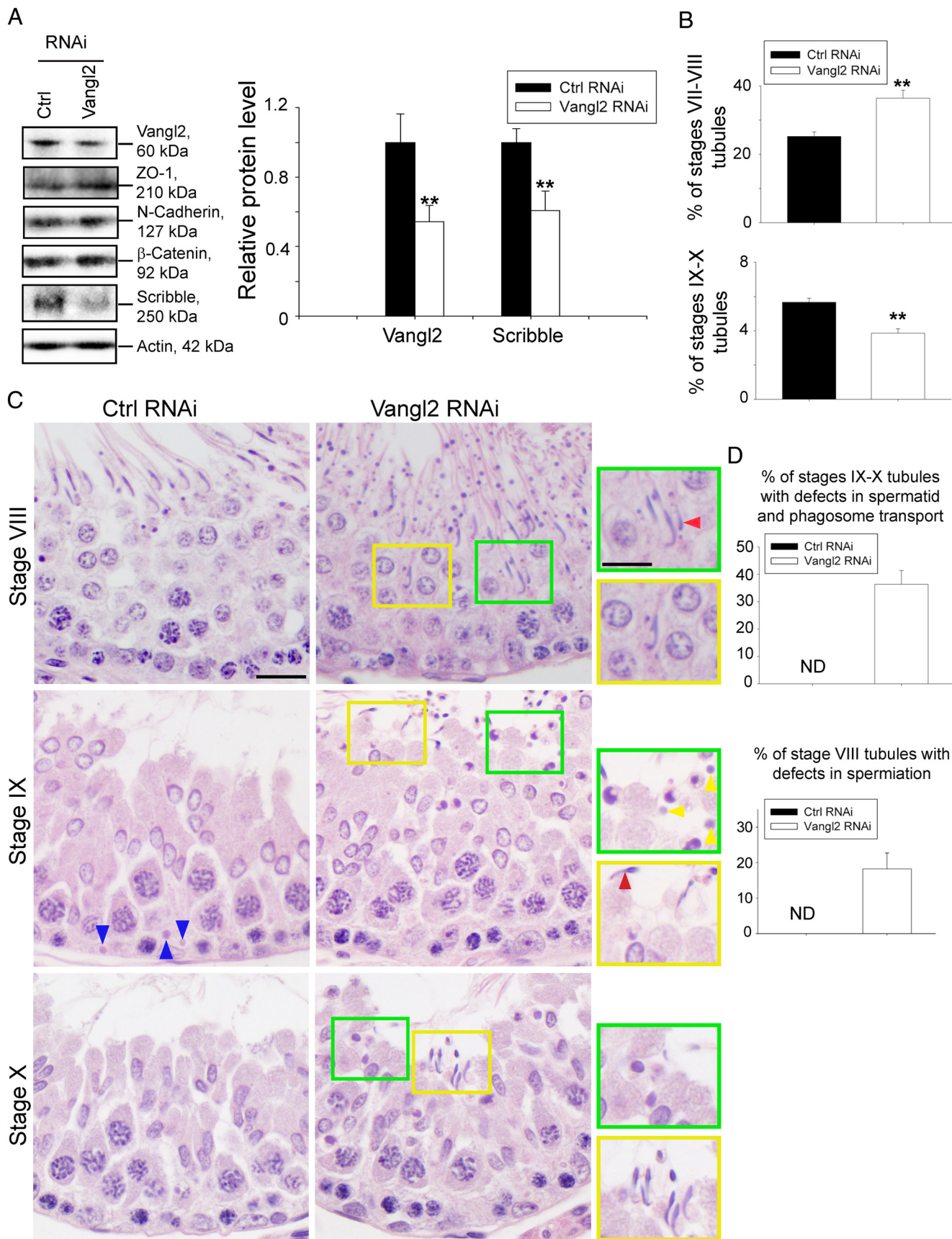


Figure 6. KD of Vangl2 in vivo affects germ cell and phagosome transport. Adult rats received intratesticular injections of Vangl2-specific siRNA duplexes vs nontargeting negative control siRNA duplexes for Vangl2 KD. Six rats were euthanized by CO₂ asphyxiation 3 days after the last transfection, and testes were

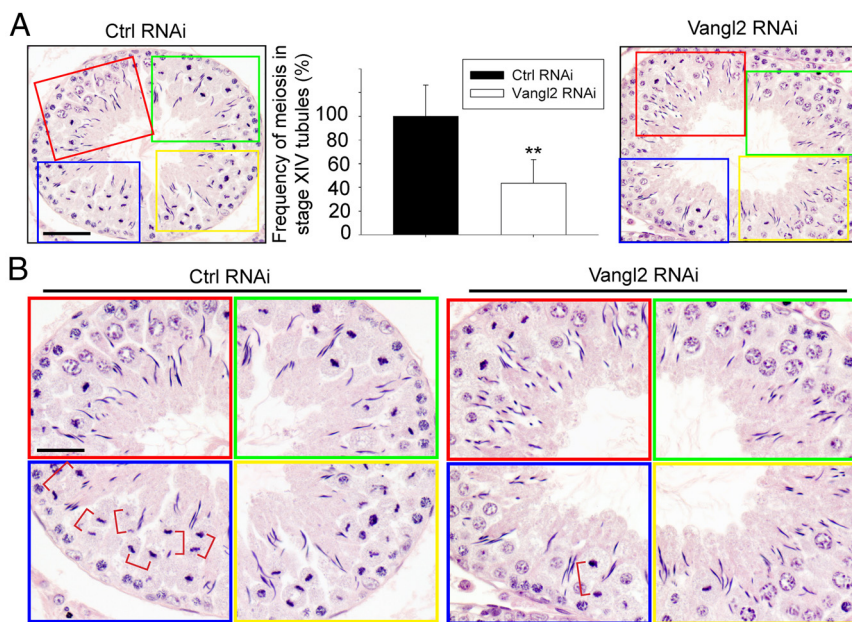


Figure 7. KD of Vangl2 in vivo perturbs meiosis. Effects of Vangl2 KD on meiosis were monitored by scoring the frequency of meiosis in stage XIV tubules. A, Control rat testes transfected with nontargeting control siRNA duplexes had approximately 30 meiotic cells as shown in the boxed areas of red, green, blue, and yellow, which were enlarged and shown in the bottom panel. Vangl2 KD reduced this frequency by at least 60%, as noted in the right panel, and these findings were summarized in the bar graph shown in the middle panel. Each bar is a mean \pm SD of three rats. **, $P < .05$ by Student's t test. Scale bar, 80 μ m, which applies to the other micrograph. B, Magnified images of the boxed colored areas shown in panel A, depicting the frequencies of meiosis. Meiotic cells at the anaphase or telophase were noted in red brackets. Scale bar, 50 μ m, which applies to other micrographs.

Figure 6. (Continued). removed for experiments. A, Immunoblotting using lysates of testes, illustrating the KD of Vangl2 had no off-target effects on other BTB-associated proteins except a down-regulation of Scribble, consistent with in vitro studies shown in Figure 3. Histogram on the right panel summarizes the immunoblotting results. Each bar is a mean \pm SD of three rat testes. **, $P < .01$ by Student's t test. B, Defects in spermatogenesis were noted in which the frequency (percentage) of stages VII–VIII and IX–X tubules was increased and decreased, respectively, due to defects in spermatid transport. The percentage of VII–VIII and IX–X tubules found in the control rat testes was consistent with results of an earlier report (67). C, Hematoxylin and eosin staining of paraffin sections of testes. Whereas elongated spermatids near the lumen edge were induced to undergo spermiation in stage VI–VII tubules, spermatids that were found deep inside the adluminal compartment of the epithelium failed to be transported to the luminal edge because step 19 spermatids were persistently found trapped inside the epithelium as noted in stage VIII tubules, and some of these spermatids had defects in polarity in which their heads were pointing 90°–180° away from the basement membrane (see red arrowhead). Step 19 spermatids remained to be seen in stage IX and even X tubules when step 9 and 10 spermatids were developed in IX and X tubules, respectively. Also, phagosomes that should have been transported to the base of the epithelium in stage IX tubules (see blue arrowheads in control testes) as reported (50) were also found near the luminal edge (see yellow arrowheads in green boxed area), illustrating defects in phagosome transport, and defects in polarity were also noted (see red arrowhead). Some areas were boxed in yellow or green and magnified and shown on the right panel. Scale bar, 15 μ m; scale bar in inset, 15 μ m, which applies to other micrographs and insets. D, Histogram summarizing results of stages IX–X tubules and stage VIII tubules with defects vs control testes. ND, not detectable. Each bar is a mean \pm SD of three rat testes.

Basal ES

A KD of Vangl2 in the testis in vivo induced changes in the F-actin organization at the BTB as noted in Figure 9A in which F-actin remained robustly expressed in stage VIII tubules when it should have been subsided as in control testes. This robust expression of F-actin is likely mediated by an up-regulation of Eps8, concomitant with a down-regulation of Arp3 at the BTB after Vangl2 KD (Figure 9A). The net result of these changes thus promoted the retention of ZO-1 and N-cadherin at the BTB (Figure 9B). Scribble expression at the BTB was considerably down-regulated (Figure 9B).

Discussion

During spermatogenesis, spermatids are properly arranged in the seminiferous epithelium to allow the maximal number of spermatids to be supported by a fixed number

of Sertoli cells (for a review, see reference 25). Studies have shown that the Par- (21) and Scribble (23)-based polarity protein complexes are crucial to confer Sertoli cell and spermatid polarity to facilitate their orderly but dynamic orientation (19, 68). Studies have shown that PCP proteins are crucial to confer directional cell polarity within the plane of an epithelium such as the orderly arrangement of hair on a fly wing and stereocilia in the inner ear of mammals analogous to polarized spermatid across the plane of the epithelium of a seminiferous tubule (for a review, see reference 12). Because ES is an F-actin-rich ultrastructure supported by bundles of actin microfilaments and the organization of these actin bundles changes rapidly in response to stages of the epithelial cycle to facilitate spermatid transport while maintaining spermatid and Sertoli cell PCP and testis was shown herein to express many PCP proteins, we thus sought to explore whether Vangl2 is involved in regulating actin microfilaments at the basal and apical ES. Indeed, a knockdown of Vangl2 in Sertoli cells by RNAi was found to promote TJ function through a recruitment of basal ES/BTB protein N-cadherin and TJ proteins claudin 11 and ZO-1 to the Sertoli cell-cell interface. These findings are consistent with the phenotypes observed in the testis in vivo after Vangl2 KD. On

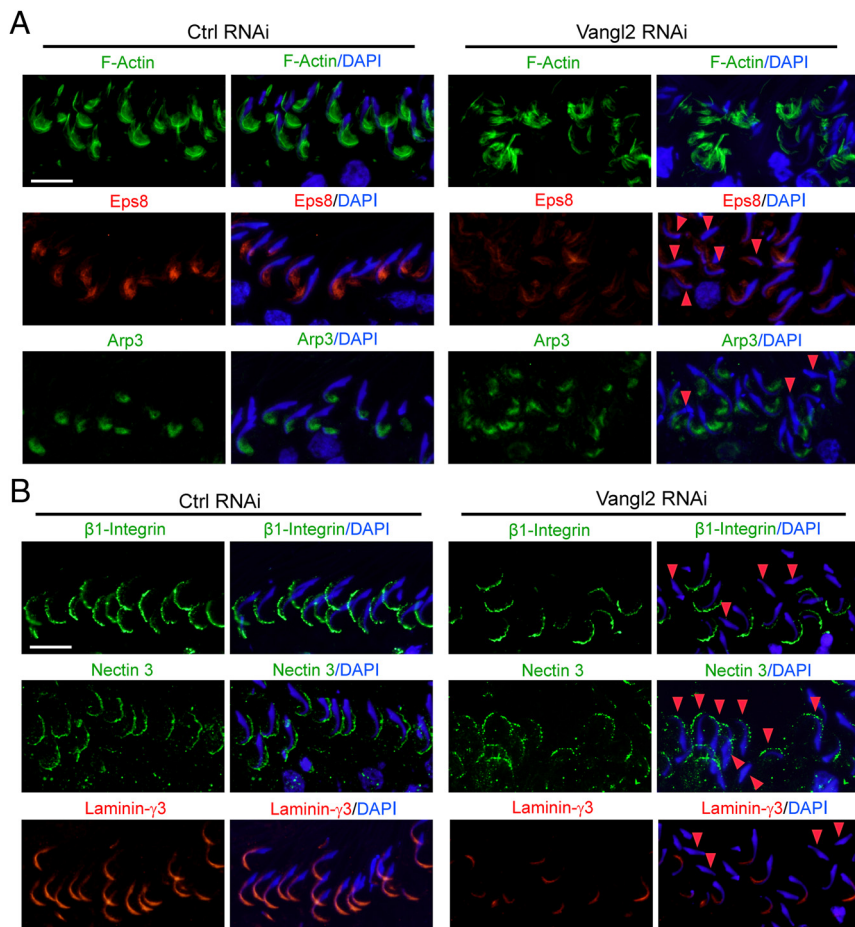


Figure 8. Vangl2 KD in the testis in vivo alters actin organization at the apical ES via changes in the spatiotemporal expression of Eps8 and Arp3 that impairs adhesion protein localization, impairing spermatid polarity and adhesion. A, Vangl2 KD by RNAi caused a disorganization of F-actin (green) at the apical ES, in which F-actin no longer expressed abundantly near the tip and the concave (ventral) side of the spermatid head, resulting from changes in the spatiotemporal expression of Eps8 (red) and Arp3 (green). In spermatids that had defects in polarity (see red arrowheads) in which their heads no longer pointed toward the basement membrane but deviated by at least 90° away from the intended orientation, considerably reduced Eps8 and/or Arp3 was detected. Scale bar, 50 μ m, which applies to other micrographs. B, Changes in the F-actin organization led to changes in the distribution of apical ES adhesion proteins β 1-Integrin (green, specific to Sertoli cells), nectin-3 (green, specific to spermatids), and laminin- γ 3 chain (red, specific to spermatids) because these proteins use F-actin for attachment. It was noted that these apical ES adhesion proteins no longer tightly associated with apical ES but considerably diminished in particular in spermatids displaying defects in polarity (see red arrowheads). Scale bar, 50 μ m, which applies to other micrographs.

the other hand, overexpression of Vangl2 in Sertoli cells perturbed the TJ barrier by causing mislocalization of basal ES/BTB protein N-cadherin as well as TJ proteins claudin 11 and ZO-1 at the cell-cell interface in which these proteins were internalized and relocated into the cell cytosol. These findings are also consistent with reports that Vangl2 exerts its effects via its interaction with N-cadherin or E-cadherin (38–40), likely modulating Rab5 (a GTPase and a member of the Ras superfamily of monomeric G proteins) and dynamin-mediated endocytosis and intracellular protein trafficking (40).

Scribble, a cell polarity protein known to regulate Sertoli cell F-actin organization (23) and localized at the Sertoli cell-cell interface at the BTB (23) as shown herein, was found to be down-regulated considerably after Vangl2 KD in Sertoli cells that led to a tightening of the TJ barrier. This observation is in agreement with findings in vivo after Vangl2 KD in the testis when ZO-1 and N-cadherin were found to be recruited and retained to the Sertoli cell-cell interface at the basal ES/BTB, concomitant with a considerable down-regulation of Scribble at the site. These findings are also consistent with our earlier study in which a triple KD of Scribble and its partner proteins Lgl2 (Lethal giant larvae 2) and Dlg1 (Discs large 1 tumor suppressor) was shown to promote the Sertoli cell TJ barrier in vitro by inducing recruitment and retention of occludin and F-actin at the basal ES/BTB in vivo (23). Also, overexpression of Vangl2 in Sertoli cells that perturbed the TJ barrier was found to promote the retention of Scribble at the cell-cell interface, leading to an increase in internalization of claudin-11, ZO-1, and N-cadherin from cell cortical zone into the cytosol. In addition to a polarity protein, Scribble is also a PCP protein that works in concert with Vangl2 to confer PCP (69, 70). In this context, it is of interest to note that Scribble KO also led to neural tube defects in mice (69, 71), similar to defects found in Vangl2 inactivated mice (27, 33) or Vangl2 mutants (73), supporting the notion that these two proteins are working in concert to support cell and/or tissue functions, such as during brain development. Thus, it is not unusual to detect structural interaction between Scribble and Vangl2 in the testis as reported herein, considering that Vangl2 contains a PDZ (post-dynaptic density protein 95, *Drosophila* discs large protein, zonula occludens 1) domain at its C terminus that mediates Scribble interaction (70, 72) because Scribble has four PDZ domains (74).

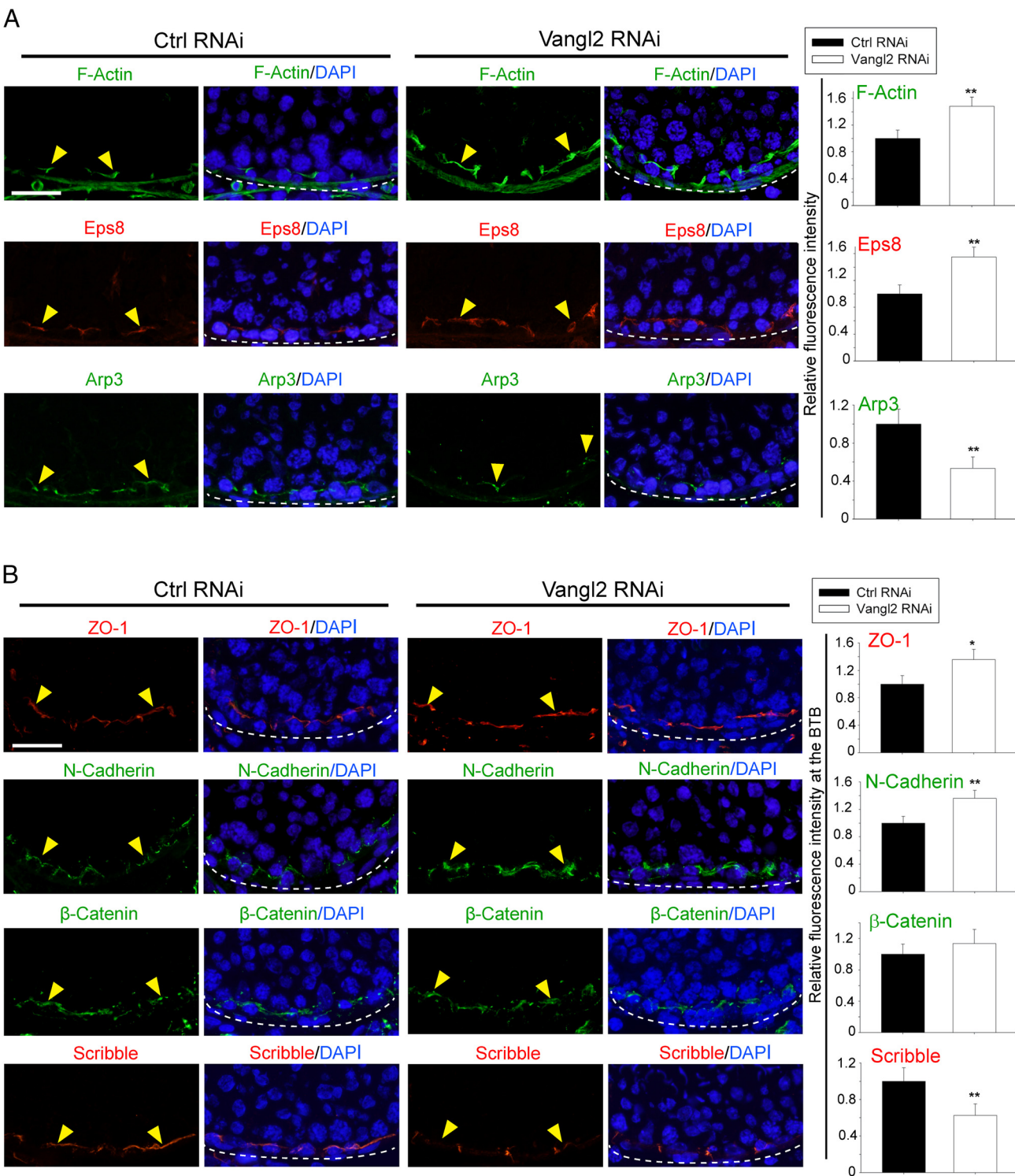


Figure 9. Vangl2 KD in the testis in vivo impedes BTB dynamics. A, Vangl2 KD in the testis in vivo led to a persistent presence of F-actin in stage VIII tubules when F-actin should have been transiently reduced to facilitate the transport of preleptotene spermatocytes across the BTB (annotated by yellow arrowheads) as seen in control testes. The basement membrane, adjacent to the BTB, is annotated by a dashed white line. These changes in F-actin organization was supported by an alteration on the spatiotemporal expression of Eps8 and Arp3 at the site, which included a persistent presence of Eps8, but a concomitant disappearance of Arp3 so that actin microfilaments remained in a bundled configuration conferred by Eps8. Scale bar, 60 μ m, which applies to other micrographs. Histograms on the right panel are a summary of the data shown in the left panel. Each bar is a mean \pm SD of three rats. **, $P < .01$ by Student's t test. B, The persistent presence of F-actin at the BTB thus supported the recruitment of ZO-1 and N-cadherin, but not β -catenin, to the BTB (annotated by yellow arrowheads), and the basement membrane is annotated by a dashed white line. Also, a down-regulation of Scribble at the BTB was noted, consistent with earlier findings based on a KD of Scribble polarity complex module in the rat testis (23). Scale bar, 60 μ m, which applies to other micrographs. Histograms on the right panel are a summary of the data shown in the left panel. Each bar is a mean \pm SD of three rats. *, $P < .05$, **, $P < .01$ by Student's t test.

It is likely that Scribble and Vangl2 are involved in regulating endocytic vesicle-mediated protein trafficking through their effects on actin microfilament organization in Sertoli cells because the silencing of either protein by RNAi promotes Sertoli cell TJ-permeability barrier function via an increase in actin microfilaments at the cell cortical zone (23) as noted herein. This notion is supported by two recent reports illustrating that Vangl2 binds to N- or E-cadherin in epithelial cells, enhancing cadherin endocytosis mediated by a small GTPase Rab5 and dynamin (39, 40), and studies have shown that endocytic vesicle trafficking is an actin cytoskeleton-dependent event (75, 76). Furthermore, as noted herein, a KD of Vangl2 in Sertoli cells *in vitro* propelled actin microfilaments to be aligned at the Sertoli cell cortical zone with an overall decline in actin bundling activity; the increased actin microfilaments at the cell-cell interface thus promote the TJ-barrier function, which also induce recruitment and retention of claudin 11/ZO-1 and N-cadherin at the cell cortical zone. These observations were consistent when Vangl2 in the testis was KD, which led to considerable down-regulation of Scribble expression at the basal ES/BTB, concomitant with the retention of F-actin, leading to recruitment of ZO-1 and N-cadherin to the site. Consistent with these findings, overexpression of Vangl2 in Sertoli cells *in vitro* led to a disorganization of actin microfilaments cell cytosol, even though the overall actin bundling activity was induced, probably because the microfilaments near the cell-cell interface were found to be truncated. These changes thus destabilized the TJ barrier due to an increase in internalization of claudin 11, ZO-1, and N-cadherin from cell surface into the cell cytosol, which was mediated by changes in the spatial expression of actin-regulatory proteins Arp3 and Eps8.

In summary, PCP protein Vangl2 plays a significant role in regulating BTB integrity, spermatid (and phagosome) transport, and spermatid polarity, likely by working in concert with Scribble via their effects on actin microfilament organization.

Acknowledgments

We thank Dr Ka-wai Mok for his helpful discussion during the cloning of the full-length Vangl2 cDNA and his advice on the RNA interference experiments. We also thank the support of a Hong Kong University Postgraduate Research Student Award (to H.C.).

Address all correspondence and requests for reprints to: C. Yan Cheng, PhD, Senior Scientist, The Mary M. Wohlford Laboratory for Male Contraceptive Research, Center for Biomedical Research, Population Council, 1230 York Ave, New York, NY

10065. E-mail: y-cheng@popcbr.rochester.edu; or ccheng@mail.rochester.edu.

This work was supported by Grant R01 HD056034 (to C.Y.C.) and Grant U54 HD029990, Project 5 (to C.Y.C.) from the National Institutes of Health, *Eunice Kennedy Shriver National Institute of Child Health and Human Development*, National Natural Science Foundation of China/Research Grants Council (NSFC/RGC) Joint Research Scheme (N_HKU 717/12 to W.M.L.), General Research Fund from RGC (771513 to W.M.L.), and CRCG Seed Funding, University of Hong Kong (to W.M.L.).

Disclosure Summary: The authors have nothing to disclose.

References

- Wallingford JB, Fraser SE, Harland RM. Convergent extension: the molecular control of polarized cell movement during embryonic development. *Dev Cell*. 2002;2:695–706.
- Sokol SY. Spatial and temporal aspects of Wnt signaling and planar cell polarity during vertebrate embryonic development. *Semin Cell Dev Biol*. 2015;42:78–85.
- Galic M, Matis M. Polarized trafficking provides spatial cues for planar cell polarization within a tissue. *Bioessays*. 2015;37:678–686.
- Davenport D. (The cell biology of planar cell polarity.) *J Cell Biol*. 2014;207:171–179.
- Tada M, Kai M. Planar cell polarity in coordinated and directed movements. *Curr Top Dev Biol*. 2012;101:77–110.
- Munoz-Soriano V, Belacortu Y, Paricio N. Planar cell polarity signaling in collective cell movements during morphogenesis and disease. *Curr Genomics*. 2012;13:609–622.
- Simons M, Mlodzik M. Planar cell polarity signaling: from fly development to human disease. *Annu Rev Genet*. 2008;42:517–540.
- Tissir F, Goffinet AM. Shaping the nervous system: role of the core planar cell polarity genes. *Nat Rev Neurosci*. 2013;14:525–535.
- Seo JH, Ziber Y, Babayeva S, et al. Mutations in the planar cell polarity gene, Fuzzy, are associated with neural tube defects in humans. *Hum Mol Genet*. 2011;20:4324–4333.
- Carroll TJ, Yu J. The kidney and planar cell polarity. *Curr Top Dev Biol*. 2012;101:185–212.
- Ezan J, Montcouquiol M. Revisiting planar cell polarity in the inner ear. *Semin Cell Dev Biol*. 2013;24:499–506.
- May-Simera H, Kelley MW. Planar cell polarity in the inner ear. *Curr Top Dev Biol*. 2012;101:111–140.
- Tellkamp F, Vorhagen S, Niessen CM. Epidermal polarity genes in health and disease. *Cold Spring Harb Perspect Biol*. 2014;4:a015255.
- Ren DD, Kelly M, Kim SM, Grimsley-Myers CM, Chi FL, Chen P. Testin interacts with vangl2 genetically to regulate inner ear sensory cell orientation and the normal development of the female reproductive tract in mice. *Dev Dyn*. 2013;242:1454–1465.
- Henderson DJ, Chaudhry B. Getting to the heart of planar cell polarity signaling. *Birth Defects Res A Clin Mol Teratol*. 2011;91:460–467.
- Eaton S, Martrin-Belmonte F. Cargo sorting in the endocytic pathway: a key regulator of cell polarity and tissue dynamics. *Cold Spring Harb Perspect Biol*. 2014;6:a016899.
- Luga V, Wrana JL. Tumor-stroma interaction: revealing fibroblast-secreted exosomes as potent regulators of Wnt-planar cell polarity signaling in cancer metastasis. *Cancer Res*. 2013;73:6843–6847.

18. Adler PN. The frizzled/stan pathway and planar cell polarity in the *Drosophila* wing. *Curr Top Dev Biol.* 2012;101:1–31.
19. Wong EWP, Cheng CY. Polarity proteins and cell-cell interactions in the testis. *Int Rev Cell Mol Biol.* 2009;278:309–353.
20. Wong EWP, Mruk DD, Cheng CY. Biology and regulation of ectoplasmic specialization, an atypical adherens junction type, in the testis. *Biochem Biophys Acta.* 2008;1778:692–708.
21. Wong EWP, Mruk DD, Lee WM, Cheng CY. Par3/Par6 polarity complex coordinates apical ectoplasmic specialization and blood-testis barrier restructuring during spermatogenesis. *Proc Natl Acad Sci USA.* 2008;105:9657–9662.
22. Wong EWP, Sun S, Li MWM, Lee WM, Cheng CY. 14-3-3 protein regulates cell adhesion in the seminiferous epithelium of rat testes. *Endocrinology.* 2009;150:4713–4723.
23. Su WH, Wong EWP, Mruk DD, Cheng CY. The Scribble/Lgl/Dlg polarity protein complex is a regulator of blood-testis barrier dynamics and spermatid polarity during spermatogenesis. *Endocrinology.* 2012;153:6041–6053.
24. Assemat E, Bazellieres E, Pallesi-Pocachard E, Le Bivic A, Massey-Harroche D. Polarity complex proteins. *Biochim Biophys Acta.* 2008;1778:614–630.
25. Cheng CY, Mruk DD. The blood-testis barrier and its implication in male contraception. *Pharmacol Rev.* 2012;64:16–64.
26. Taylor J, Abramova N, Charlton J, Adler PN. Van Gogh: a new *Drosophila* tissue polarity gene. *Genetics.* 1998;150:199–210.
27. Kibar Z, Vogan KJ, Groulx N, Justice MJ, Underhill DA, Gros P. Ltap, a mammalian homolog of *Drosophila* strabismus/Van Gogh, is altered in the mouse neural tube mutant Loop-tail. *Nat Genet.* 2001;28:251–255.
28. Merello E, Mascelli S, Raso A, et al. Expanding the mutational spectrum associated to neural tube defects: literature revision and description of novel VANGL1 mutations. *Birth Defects Res A Clin Mol Teratol.* 2015;103:51–61.
29. Iliescu A, Gravel M, Horth C, Gros P. Independent mutations at Arg181 and Arg274 of Vangl proteins that are associated with neural tube defects in humans decrease protein stability and impair membrane targeting. *Biochemistry.* 2014;53:5356–5364.
30. Kibar Z, Torban E, McDermid JR, et al. Mutations in VANGL1 associated with neural-tube defects. *N Engl J Med.* 2007;356:1432–1437.
31. Kibar Z, Salem S, Bosoi CM, et al. Contribution of VANGL2 mutations to isolated neural tube defects. *Clin Genet.* 2011;80:76–82.
32. Lei YP, Zhang T, Li H, Wu BL, Jin L, Wang HY. VANGL2 mutations in human cranial neural-tube defects. *N Engl J Med.* 2010;362(23):2232–2235.
33. Yin H, Copley CO, Goodrich LV, Deans MR. Comparison of phenotypes between different vangl2 mutants demonstrates dominant effects of the Looptail mutation during hair cell development. *PLoS One.* 2012;7:e31988.
34. Yates LL, Papakrivopoulou J, Long DA, et al. The planar cell polarity gene Vangl2 is required for mammalian kidney-branching morphogenesis and glomerular maturation. *Hum Mol Genet.* 2010;19:4663–4676.
35. Song H, Jianxin H, Chen W, et al. Planar cell polarity breaks bilateral symmetry by controlling ciliary positioning. *Nature.* 2010;466:378–383.
36. Torban E, Patenaude AM, Leclerc S, et al. Genetic interaction between members of the Vangl family causes neural tube defects in mice. *Proc Natl Acad Sci USA.* 2008;105:3449–3454.
37. Hatakeyama J, Wald JH, Printsev I, Ho HY, Carraway KL 3rd. Vangl1 and Vangl2: planar cell polarity components with a developing role in cancer. *Endocr Relat Cancer* 2014;21:R345–R356.
38. Rocque BL, Babayeva S, Li J, et al. Deficiency of the planar cell polarity protein Vangl2 in podocytes affects glomerular morphogenesis and increases susceptibility to injury. *J Am Soc Nephrol.* 2015;26:576–586.
39. Nagaoka T, Ohashi R, Inutsuka A, et al. The Wnt/planar cell polarity pathway component Vangl2 induces synapse formation through direct control of N-cadherin. *Cell Rep.* 2014;6:916–927.
40. Nagaoka T, Inutsuka A, Begum K, Bin Hafiz K, Kishi M. Vangl2 regulates E-cadherin in epithelial cells. *Sci Rep.* 2014;4:6940.
41. Lindqvist M, Horn Z, Bryja V, et al. Vang-like protein 2 and Rac1 interact to regulate adherens junctions. *J Cell Sci.* 2010;123:472–483.
42. Mruk DD, Cheng CY. An *in vitro* system to study Sertoli cell blood-testis barrier dynamics. *Methods Mol Biol.* 2011;763:237–252.
43. Li N, Mruk DD, Wong CK, Lee WM, Han D, Cheng CY. Actin-bundling protein plastin 3 is a regulator of ectoplasmic specialization dynamics during spermatogenesis in the rat testis. *FASEB J.* 2015;29:3788–3805.
44. Lie PPY, Mruk DD, Mok KW, et al. Focal adhesion kinase-Tyr⁴⁰⁷ and -Tyr³⁹⁷ exhibit antagonistic effects on blood-testis barrier dynamics in the rat. *Proc Natl Acad Sci USA.* 2012;109:12562–12567.
45. Mok KW, Mruk DD, Cheng CY. rpS6 regulates blood-testis barrier dynamics through Akt-mediated effects on MMP-9. *J Cell Sci.* 2014;127:4870–4882.
46. Mok KW, Mruk DD, Silvestrini B, Cheng CY. rpS6 regulates blood-testis barrier dynamics by affecting F-actin organization and protein recruitment. *Endocrinology.* 2012;153:5036–5048.
47. Yan HHN, Cheng CY. Blood-testis barrier dynamics are regulated by an engagement/disengagement mechanism between tight and adherens junctions via peripheral adaptors. *Proc Natl Acad Sci USA.* 2005;102:11722–11727.
48. Ip CK, Cheung AN, Ngan HY, Wong AS. p70 S6 kinase in the control of actin cytoskeleton dynamics and directed migration of ovarian cancer cells. *Oncogene.* 2011;30:2420–2432.
49. Xiao X, Mruk DD, Lee WM, Cheng CY. c-Yes regulates cell adhesion at the blood-testis barrier and the apical ectoplasmic specialization in the seminiferous epithelium of rat testes. *Int J Biochem Cell Biol.* 2011;43:651–665.
50. Clermont Y, Morales C, Hermo L. Endocytic activities of Sertoli cells in the rat. *Ann NY Acad Sci.* 1987;513:1–15.
51. Giese AP, Ezan J, Wang L, et al. Gipc1 has a dual role in Vangl2 trafficking and hair bundle integrity in the inner ear. *Development.* 2012;139:3775–3785.
52. Lie PPY, Chan AYN, Mruk DD, Lee WM, Cheng CY. Restricted Arp3 expression in the testis prevents blood-testis barrier disruption during junction restructuring at spermatogenesis. *Proc Natl Acad Sci USA.* 2010;107:11411–11416.
53. Lie PPY, Mruk DD, Lee WM, Cheng CY. Epidermal growth factor receptor pathway substrate 8 (Eps8) is a novel regulator of cell adhesion and the blood-testis barrier integrity in the seminiferous epithelium. *FASEB J.* 2009;23:2555–2567.
54. Vogl AW, Young JS, Du M. New insights into roles of tubulobulbar complexes in sperm release and turnover of blood-testis barrier. *Int Rev Cell Mol Biol.* 2013;303:319–355.
55. Cheng CY, Mruk DD. A local autocore axis in the testes that regulates spermatogenesis. *Nat Rev Endocrinol.* 2010;6:380–395.
56. O'Donnell L, Nicholls PK, O'Bryan MK, McLachlan RI, Stanton PG. Spermiation: the process of sperm release. *Spermatogenesis.* 2011;1:14–35.
57. Vogl AW, Vaid KS, Guttman JA. The Sertoli cell cytoskeleton. *Adv Exp Med Biol.* 2008;636:186–211.
58. Qian X, Mruk DD, Cheng YH, et al. Actin binding proteins, spermatid transport and spermiation. *Semin Cell Dev Biol.* 2014;30:75–85.
59. Lie PPY, Cheng CY, Mruk DD. Cross talk between desmoglein-2/desmocollin-2/Src kinase and coxsackie and adenovirus receptor/ZO-1 protein complexes, regulates blood-testis barrier dynamics. *Int J Biochem Cell Biol.* 2010;42:975–986.
60. Li MWM, Mruk DD, Lee WM, Cheng CY. Disruption of the blood-testis barrier integrity by bisphenol A *in vitro*: Is this a suitable model

- for studying blood-testis barrier dynamics? *Int J Biochem Cell Biol.* 2009;41:2302–2314.
61. Pebernard S, Iggo RD. Determinants of interferon-stimulated gene induction by RNAi vectors. *Differentiation.* 2004;72:103–111.
 62. Meng Z, Zu Y, Wu J, et al. Inhibition of hepatitis B virus gene expression and replication by endoribonuclease-prepared siRNA. *J Virol Methods.* 2008;150:27–33.
 63. Kaucka M, Petersen J, Janovska P, et al. Asymmetry of VANGL2 in migrating lymphocytes as a tool to monitor activity of the mammalian WNT/planar cell polarity pathway. *Cell Commun Signal.* 2015; 13:2.
 64. Babayeva S, Zilber Y, Torban E. Planar cell polarity pathway regulates actin rearrangement, cell shape, motility, and nephrin distribution in podocytes. *Am J Physiol Renal Physiol.* 2011;300:F546–F560.
 65. Mruk DD, Cheng CY. Sertoli-Sertoli and Sertoli-germ cell interactions and their significance in germ cell movement in the seminiferous epithelium during spermatogenesis. *Endocr Rev.* 2004;25:747–806.
 66. Cheng CY, Mruk DD. Regulation of spermiogenesis, spermiation and blood-testis barrier dynamics: novel insights from studies on Eps8 and Arp3. *Biochem J.* 2011;435:553–562.
 67. Hess RA, Schaeffer DJ, Eroschenko VP, Keen JE. Frequency of the stages of the cycle of the seminiferous epithelium in the rat. *Biol Reprod.* 1990;43:517–524.
 68. Su WH, Mruk DD, Wong EWP, Lui WY, Cheng CY. Polarity protein complex Scribble/Lgl/Dlg and epithelial cell barriers. *Adv Exp Med Biol.* 2012;763:149–170.
 69. Montcouquiol M, Rachel RA, Lanford PJ, Copeland NG, Jenkins NA, Kelley MW. Identification of Vangl2 and Scrb1 as planar polarity genes in mammals. *Nature.* 2003;423:173–177.
 70. Kallay LM, McNickle A, Brennwald PJ, Hubbard AL, Bralteman LT. Scribble associates with two polarity proteins, Lgl2 and Vangl2, via distinct molecular domains. *J Cell Biochem.* 2006; 99:647–664.
 71. Murdoch JN, Henderson DJ, Doudney K, et al. Disruption of scribble (Scrb1) causes severe neural tube defects in the circletail mouse. *Hum Mol Genet.* 2003;12:87–98.
 72. Montcouquiol M, Sans N, Huss D, et al. Asymmetric localization of Vangl2 and Fz3 indicate novel mechanisms for planar cell polarity in mammals. *J Neurosci.* 2006;26:5265–5275.
 73. Murdoch JN, Rachel RA, Shah S, et al. Circletail, a new mouse mutant with severe neural tube defects: chromosomal localization and interaction with the loop-tail mutation. *Genomics.* 2001;78:55–63.
 74. Nakagawa S, Yano T, Nakagawa K, et al. Analysis of the expression and localisation of a LAP protein, human scribble, in the normal and neoplastic epithelium of uterine cervix. *Br J Cancer.* 2004;90:194–199.
 75. Loebrich S. The role of F-actin in modulating clathrin-mediated endocytosis: lesions from neurons in health and neuropsychiatric disorder. *Commun Integr Biol.* 2014;7:e28740.
 76. Granger E, McNee G, Allan V, Woodman P. The role of the cytoskeleton and molecular motors in endosomal dynamics. *Semin Cell Dev Biol.* 2014;31:20–29.